Available online at www.sciencedirect.com
ScienceDirect
Developmental Biology 315 (2008) 1 – 17
DEVELOPMENTAL BIOLOGY
www.elsevier.com/developmentalbiology

Alterations of the cytoskeleton in all three embryonic lineages contribute to the epiboly defect of Pou5f1/Oct4 deficient MZ*spg* zebrafish embryos

Martina Lachnit, Esther Kur, Wolfgang Driever *

Department of Developmental Biology, Institute Biology 1, University of Freiburg, 79104 Freiburg, Germany

Received for publication 16 June 2007; revised 3 October 2007; accepted 5 October 2007
Available online 13 October 2007

Abstract

Pou5f1/Oct4 is a transcription factor required for pluripotency of embryonic stem cells in mammals. Zebrafish *pou5f1* deficient maternal and zygotic *spiel ohne grenzen* (MZ*spg*) mutant embryos develop severe gastrulation defects, are dorsalized, and defective in endoderm formation. Here we analyze in detail gastrulation defects, which are manifested by a severe delay in epiboly progression. All three embryonic lineages in MZ*spg* embryos behave abnormally during epiboly: the yolk cell forms an altered array of cortical microtubules and F-Actin, with large patches of microtubule free areas; the enveloping layer (EVL) is delayed in the coordinated cell shape changes of marginal cells, that may be mediated by F-Actin; the deep layer cells (DEL), forming the embryo proper, are non-autonomously affected in their motility and do not enter the space opening by epiboly of the EVL. Analysis of adhesiveness as well as high resolution *in vivo* time lapse image analysis of DEL cells suggests changed adhesive properties and inability to migrate properly on EVL and yolk syncytial layer (YSL) surfaces. Our data further reveal that during epiboly the EVL may actively probe the YSL by filopodia formation, rather than just being passively pulled vegetalwards. Our findings on the effect of Pou5f1 on cell behavior may be relevant to understand stem cell behavior and tumorigenesis involving Pou5f1.

Keywords: Pou5f1; Oct4; *Spiel ohne grenzen* (*spg*); Zebrafish; Epiboly; Gastrulation; Cell migration

Introduction

Pou5f1, a POU domain transcription factor better known as Oct4, is critical for maintenance of pluripotency and self-renewal of inner cell mass cells and germ line development in mice (Nichols et al., 1998; Ovitt and Scholer, 1998; Kehler et al., 2004; Boiani et al., 2005; Boiani and Scholer, 2005). The activity of Pou5f1 in maintaining pluripotency is mediated through a complex transcriptional network (Boyer et al., 2005; Ivanova et al., 2006; Loh et al., 2006), but Pou5f1 also contributes in a concentration-dependent manner to specific lineage decisions. This includes the decision between trophectoderm and inner cell mass, and later induction of endoderm development (Niwa et al., 2000; Pesce and Scholer, 2001; Alarcon and Marikawa, 2004; Niwa, 2007). It has been suggested that Pou5f1 may also control cell proliferation and cell behavior, as Pou5f1 ectopic expression appears to induce epithelial dysplasia (Hochedlinger et al., 2005).

A potential role of Pou5f1 in the control of adhesive and migratory properties of cells during early embryogenesis is difficult to analyze in mammals, due to inaccessibility of postimplantation gastrula stages. The zebrafish represents an evolutionarily simpler vertebrate model organism, where all blastula and gastrula stages can be analyzed easily (Kimmel et al., 1995), and therefore provides an appropriate tool to study *in vivo* regulatory roles of Pou5f1 in the control of morphogenetic movements during gastrulation. Similar to mammals, the zebrafish *pou5f1* orthologue is expressed during oogenesis, with maternal mRNA deposited into the ooccyte. After activation of the zygotic genome at midblastula transition (MBT), *pou5f1* is broadly expressed in all cells. Later *pou5f1* expression is restricted to the embryonic epiblast, and turned off in the extraembryonic structures, *env*eloping *l*ayer (EVL), *y*olk *c*ytoplasmic *l*ayer, and *y*olk *s*yncytial *l*ayer (YCL and YSL), as well as in the embryonic hypoblast (Takeda et al., 1994; Howley

* Corresponding author. Fax: +49 761 203 2597.
E-mail address: driever@biologie.uni-freiburg.de (W. Driever).

0012-1606/$ - see front matter © 2007 Elsevier Inc. All rights reserved.
doi:10.1016/j.ydbio.2007.10.008

and Ho, 2000). Mutations in zebrafish *pou5f1* were initially identified as the *spiel ohne grenzen* (*spg*) genetic locus (Belting et al., 2001; Burgess et al., 2002). Embryos devoid of maternal and zygotic Pou5f1 function, so-called *M*aternal and *Z*ygotic (MZ) *spg* mutant embryos, display severe phenotypes including absence of endoderm (Lunde et al., 2004; Reim et al., 2004) and abnormal gastrulation behavior (Lunde et al., 2004; Reim et al., 2004; Reim and Brand, 2006). Absence of endoderm in MZ*spg* embryos is caused by a requirement for Pou5f1 during maintenance of *sox32* and activation of *sox17* expression, downstream of Nodal signaling (Lunde et al., 2004; Reim et al., 2004). However, Nodal signaling itself and induction of mesoderm appear normal in MZ*spg* embryos. Furthermore, absence of Pou5f1 affects dorsoventral patterning: MZ*spg* embryos are dorsalized, as Pou5f1 appears to be required for normal activation of ventral expression of BMP genes (Reim and Brand, 2006). In contrast, neuroectoderm forms and is patterned along the anterioposterior axis, albeit in a compressed and distorted fashion, which may be caused by gastrulation defects (Lunde et al., 2004; Reim et al., 2004). Similarities from fish to mammals include roles of Pou5f1 in endoderm development, downregulation of Pou5f1 in extraembryonic lineages, and links to BMP signaling. Furthermore, over-expression of mouse Oct4/Pou5f1 in zygotic *spg* mutant zebrafish may rescue aspects of the mutant phenotype, indicating strong conservation of protein functions (Burgess et al., 2002).

MZ*spg* mutant embryos provide an opportunity to investigate differences in cell behavior during gastrulation in the absence of Pou5f1 activity. The rapid development and the translucent nature of the embryos enabled experiments that led to a detailed understanding of the complex morphogenetic processes driving gastrulation *in vivo* (Solnica-Krezel et al., 1995; Myers et al., 2002; Montero et al., 2003; Solnica-Krezel, 2005; Solnica-Krezel, 2006). Before MBT, cells of the zebrafish embryo are non-motile (Kane and Kimmel, 1993). Directly after MBT, the three major cell lineages of the early gastrula embryo form. Two lineages give rise to extraembryonic structures: the EVL, as outer cellular layer, and the YSL and YCL, covering the yolk cell. The third lineage, the deep cells (also termed DEL for *de*ep cell *l*ayer) will later form all three embryonic germ layers: ectoderm, endoderm, and mesoderm. One hour after MBT, doming of the yolk cell initiates epiboly, during which the blastoderm spreads vegetalwards over the yolk cell. All three early lineages, EVL, YSL, and deep cells, participate in this process (Arendt and Nubler-Jung, 1999). The second active migratory behavior during gastrulation is emboly (internalization) of cells at the margin to form the hypoblast (endoderm and mesoderm), soon followed by convergence and extension movements to establish and extend the embryonic axis. Emboly and convergence and extension progress until the end of gastrulation in parallel with epiboly. Epiboly movement is observed in all vertebrate groups to expand the blastoderm and initiate the gastrulation process (Arendt and Nubler-Jung, 1999; Solnica-Krezel, 2005), and constitutes the first active cell migration process (Kane and Kimmel, 1993). In its essence, epiboly is a phase of migratory spreading to generate a sheet of cells- and thus epiboly also occurs in mammals, even though cells do not spread over a vegetal yolk mass. The molecular control of epiboly is poorly understood, but a number of mechanisms have been implicated in orchestrating epiboly cell movement: the vegetal movement of the YSL is coordinated through microtubule arrays located within the YSL and YCL, which have been proposed to pull the EVL, being tightly attached to the YSL, vegetalwards (Strahle and Jesuthasan, 1993; Solnica-Krezel and Driever, 1994; Koeppen et al., 2006). Endocytic vesicle recycling of the YSL membrane may aid epiboly in moving membrane from the vegetal side of EVL attachment to the animal side, supporting in a treadmill-like process progression of the YSL (Betchaku and Trinkaus, 1978; Solnica-Krezel et al., 1995). Furthermore, contractile elements at the EVL margin and a punctuate Actin band within the YSL drive the late phase of epiboly (Cheng et al., 2004), possibly through coordinated epithelial cell shape changes of EVL marginal cells (Cheng et al., 2004; Koeppen et al., 2006). There is some similarity between epiboly and the purse-string mechanism proposed for dorsal closure process in *Drosophila* (Jacinto et al., 2002a,b). Recently it was reported that the EVL serves as a migration substrate for deep cells (Shimizu et al., 2005). Thus interference with epiboly progression, cellular integrity, or adhesive properties of the EVL may also result in retardation of deep cell epiboly. In fact, one of the zebrafish mutations with a severe epiboly progression phenotype, *half-baked* (*hab*), has been demonstrated to affect the *cadherin 1* (*cdh1*) gene encoding E-Cadherin (Kane et al., 2005; Shimizu et al., 2005). *cdh1* deficient embryos display a reduced radial intercalation movement of deep cells, which cause a delay in flattening of the blastoderm (Kane et al., 2005). Interestingly in MZ*cdh1* embryos, the EVL completes epiboly, but deep cells do not. The finding that in *cdh1* deficient embryos adhesion between deep cells is normal, but is disrupted between deep cells and EVL, supports the hypothesis that deep cells use E-Cadherin mediated adhesion to the EVL substrate during their vegetal progression (Shimizu et al., 2005). A number of other factors have been shown to affect cell motility in epiboly, such as Prostaglandin E2 signaling through the epinephrine receptor 4 (EP4) (Cha et al., 2006), the Rac-GAP activity protein alpha2-Chimerin (Leskow et al., 2006), and a Src kinase encoded by *angiomotin-like2* (*amotl2*) (Huang et al., 2007). However, it is still unclear how specific they function in control of epiboly progression.

In this study, we investigated *pou5f1* deficient MZ*spg* embryos in detail to identify changes in morphogenetic processes driving epiboly of all three embryonic lineages. Loss of function analysis revealed a crucial role of Pou5f1 for the cytoskeletal organization and behavior of the EVL and YSL. In *pou5f1* deficient embryos, the integrity of the large microtubule arrays located within the YSL and YCL, which have been implicated in the control of yolk syncytial nuclei (YSN) and EVL epiboly, is distorted. Furthermore, marginal cells of the EVL are delayed in their characteristic coordinated epithelial cell shape change, that may go along with an Actin mediated purse-string mechanism contributing to epiboly progression during the late phase. In addition, during the final phase of epiboly, EVL

cells of *pou5f1* deficient embryos form an excessive number of lamellipodia. We present evidence for a migratory behavior of EVL cells, as these cells form extensive filopodia in the direction of migration in a manner reminiscent of guidance cue sensing. Although deep cells are motile and show extensive protrusive behavior in MZ*spg* embryos, we can demonstrate that they have different adhesive properties from wild-type deep cells. In summary, our data demonstrate an extensive influence of Pou5f1 on cytoskeleton, cell adhesion, and cell behavior during early gastrulation. These findings may contribute to a better understanding of the role of Pou5f1 in inner cell mass and stem cell behavior of higher vertebrate systems.

Experimental procedures

Zebrafish strains and embryo culture

Fish maintenance was performed as described (Westerfield, 1994). MZspg^{m793} fish were obtained and maintained as described (Lunde et al., 2004). The spg^{m793} allele was induced in an AB strain background (Belting et al., 2001). The fish used as wild-type control were of AB or AB/TL strain. For experiments that require precise staging of embryos, *w*ild-*t*ype (WT) and MZspg^{m793} embryos were selected at the four-cell stage, and thus pools of synchronous embryos generated. Experiments were performed at 25–28 °C.

Mutant strains

Strains homozygous for spg^{m793} or spg^{hi349} (Lunde et al., 2004; Reim et al., 2004) were used to generate MZ mutant *spg* (MZ*spg*) embryos (Schier et al., 1996). spg^{m793} contains a point mutation at the splice acceptor site of intron 1 resulting in a stop codon at the beginning of exon 2, and thus in the loss of the POU domain, which confers DNA binding capacity to Pou5f1 (Schier et al., 1996; Belting et al., 2001). PCR identification of Zspg^{m793} embryos was performed as described (Belting et al., 2001). spg^{hi349} is based on a retroviral insertion in the POU-specific domain (Amsterdam and Hopkins, 1999). This integration disrupts the POU-specific domain, and truncates the protein before the POU homeodomain. Thus it is likely that this integration generates a null allele (Burgess et al., 2002).

For observation, living embryos were mounted in 2.5% methylcellulose in 0.3× Danieau's solution (1× Danieau's solution: 58 mM NaCl, 0.7 mM KCl, 0.4 mM $MgSO_4$, 0.6 mM $Ca(NO_3)_2$, 5 mM HEPES, pH 7.6) (Shih and Fraser, 1996), or in 0.3× Danieau's (yolk cell size comparison). Pictures were taken with Zeiss Axiocam MR1 camera and software using a Leica MZ APO dissecting microscope with a Plan Apo 1.6× objective.

mRNA transcription and microinjection

mRNA encoding membrane anchor tagged GFP (Jiang and Hunter, 1998) was transcribed using SP6 message machine (Ambion). Microinjection was performed as described (Westerfield, 1994).

Cytoskeletal and nuclear staining

Alexa488-Phalloidin (Molecular probes; 1:40) staining was performed as described (Cheng et al., 2004). Anti-β-Tubulin staining (antibody KMX-1 at 1:500, Chemicon) was performed as described (Gard, 1991; Solnica-Krezel and Driever, 1994). Sytox green staining: samples fixed in 4% Paraformaldehyde (PFA) were washed in PBT and incubated over night at 4 °C in 0.5 μM Sytox green (Molecular Probes) diluted in PBS, 0.1% TritonX-100 (PBT), washed in PBT and stored at 4 °C until confocal acquisition.

Confocal microscopy

Confocal images and time lapse 4D-acquisitions were made using Zeiss LSM-510 confocal microscopes (Carl Zeiss Micro Imaging, Jena) using 488 nm and 546 nm laser sources. Embryos were incubated at 28 °C using a heating unit (Zeiss) for time lapse recordings. Embryos were mounted either in 2.5% methylcellulose dissolved in 0.3× Danieau's or in 0.5–0.8% agarose dissolved in 0.3× Danieau's. Confocal acquisition parameters of fixed samples: anti-β-Tubulin/anti-mouse Alexa488 staining: Plan-Apochromat 20×/0.75, pixel size: 0.64 μs × 0.64 μs × 0.64 μs, wavelength: 488 nm, BP500-550IR, optical slice: 1.8 μm. Phalloidin staining: (1) Coordinated cell shape change of EVL cells: Plan-Apochromat 20×/0.75, pixel size: 1.27 μm × 1.27 μm × 0.9 μm, wavelength: 488 nm, BP500-550IR, optical slice: 1.8 μm. (2) EVL lamellipodia analysis: C-Apochromat 63×/1.2 W, pixel size: 0.2 μm × 0.2 μm × 0.45 μm, wavelength: 488 nm, BP500-550IR, optical slice: 3.3 μm. Sytox nuclear staining: Plan-Apochromat 20×/0.75, pixel size: 1.27 μm × 1.27 μm × 0.9 μm, wavelength: 488 nm, BP500-550IR, optical slice: 1.8 μm.

Quantification of cell number in the embryo

Wild-type and MZspg^{m793} mutant embryos were generated by *in vitro* fertilization (IVF). Time of IVF was used for precise timing of development. Embryos were incubated at 28.5 °C in a water bath and fixed in 4% PFA at exactly 4 or 5 h, respectively. Fixed embryos were dechorionated, dehydrated in MeOH overnight, rehydrated in PBT, stained with Sytox green (2 μM in PBS) for 24 h, and washed several times in PBT. For confocal analysis, embryos were mounted in 2% low melting point agarose. Confocal stacks were taken using a Zeiss Imager.Z1 with LSM 510 software. Parameters for confocal acquisition: Achroplan 10×/0.3 W Ph1, scaling: *X*: 1.46 μm, *Y*: 1.64 μm, *Z*: 0.82 μm, filter: LP 505, beam splitters: MBS: HFT488, DBS1: Mirror, DBS2: NFT 490, wave length: 488 nm, laser: 5.1%. Confocal stacks were then analyzed by Volocity software version 4.1.0 (Improvision). Volocity can identify and measure objects which are defined by threshold values for a number of classifiers. Nuclei were detected using the following classifier criteria: (1) find objects by intensity: lower threshold 104, upper threshold 255; (2) separate touching objects: object size guide 200 μm^3; (3) fill holes in objects; (4) exclude objects <100 μm^3; (5) exclude objects >4000 μm^3.

Cell transplantation assay

Transplantation of cell groups was performed as described (Reim et al., 2004). 4D confocal data were rendered using Volocity 3.6.1. (Improvision Deutschland, Tübingen, Germany). 4D-Time lapse data were exported as 8 bit TIFF image series, and re-imported into ImageJ (http://rsb.info.nih.gov/ij/). In ImageJ, single cells were tracked and velocity calculated. Velocity data of cells were averaged ($\bar{v}_n = \sum_n v/n$), standard deviation (SD), and *p*-value calculated. The results were normalized to WT data and expressed in % of the WT value set as 100%. Confocal acquisition parameters: C-Apochromat 63 × 1.2 W, pixel size: 0.45 μm × 0.45 μm × 1.15 μm, wavelength: 488 nm, 532 nm, BP505-530, LP560, optical slice: 0.6 μm.

Cell dissociation and aggregation assay

Dissociation and cultivation of cells were in principle performed as described (Montero et al., 2003; von der Hardt et al., 2007). Embryos were injected at the one cell stage either with Alexa488-dextran or Rhodamine-dextran (Invitrogen GmbH; Karlsruhe, Germany). After manual dechorionation, the embryos were transferred into 0.5 mg/ml Trypsin/0.2 mg/ml EDTA and incubated 5 min at 28 °C while shaking at 300 rpm. The reaction was then stopped by addition of fetal calf serum (PAA Lab GmbH, Cölbe, Germany). Embryos were then dissociated by resuspending through a glass Pasteur pipette 15–25 times. Cells were harvested by spinning 5 min at 500 rpm and 28 °C. The cell pellet was dispersed in L-15 medium supplemented with 0.3 mg/ml L-glutamine (Sigma-Aldrich, Munich, Germany) and plated on Petri dishes (ibidi GmbH, Martinsried, Germany) coated with a mixture of 10 μg/ml Fibronectin and a Collagen solution, added at 1:10 (purified bovine dermal Collagen, Cellon, Strassen, Luxembourg). After documentation of the dissociation efficiency, dishes were incubated at 28 °C. Aggregation of cells was analyzed by confocal microscopy (Confocal acquisition parameters: EC Plan-Neofluar 10 × 0.3, pixel size: 2.5 μm × 2.5 μm × 15 μm, wavelength: 488 nm, 543 nm, BP500-530IR, LP560, optical slice: 3 μm).

Volume measurements were performed with Volocity 4 (Improvision) software using the classification and measurement modules and the following parameters: "Find objects by intensity" for both channels (intensity thresholds adjusted for each stack), "Exclude objects by size" lower than 10 μm, "Fill holes in objects", "Color objects" uniform, "Measure objects".

To minimize potential tracer dye influence, the analysis of differences in the aggregation behavior of WT and MZ*spg*^{m793} cells was performed reciprocally with respect to the two dyes used. A total of 223 genetically heterogeneous MZ*spg*-WT clusters and 165 homogeneous WT-WT were analyzed for one dye combination, and for the reciprocal dye combination, 124 genetically heterogeneous MZ*spg*-WT and 163 homogenous WT-WT clusters were analyzed. The total amount of cells of both cell types was determined by measuring the volumes of differentially fluorescently labeled cell types within one analyzed section. We compared WT versus WT volumes of homogeneous cultures and WT versus MZ*spg* volumes of heterogeneous cultures. The difference was calculated for each comparison ($n=11$ per cluster type) and the p-value determined. In one experiment, the seeded cell number and the cell volume after 16 h of culture were not significantly different between WT and MZ*spg* cells. In a second experiment, the total volume of MZ*spg* cell was determined to be only about 65% of the total volume of the wild-type cells; however, this had no effect on relative cluster composition of heterogeneous clusters.

Analysis of filopodia formation and deep cell behavior

Embryos were labeled by microinjections at 1-cell stage with mRNA encoding membrane tagged GFP (Jiang and Hunter, 1998), supplemented with either 0.5 mM Sytox green (Invitrogen GmbH; Karlsruhe, Germany) or Alexa488 dextran (MW 10 kDa) (Invitrogen GmbH; Karlsruhe, Germany). Filopodia formation and deep cell behavior were visualized using confocal time lapse acquisition (Confocal acquisition parameters: C-Apochromat 63×1.2 W pixel size: 0.2 μm×0.2 μm, wavelength: 488 nm, BP500-550, optical slice: 0.9 μm).

Endocytic behavior at the EVL–YSL interface

Embryos were treated with 1.5% Lucifer Yellow/0.3× Danieau's as described (Solnica-Krezel and Driever, 1994). Stained live embryos were mounted in 2.5% Methylcellulose/0.3× Danieau's. Confocal acquisition parameters: Plan-Apochromat 20×0.75, pixel size: 0.3 μm×0.3 μm×0.3 μm, wavelength: 458 nm, 473–559, optical slice: 0.7 μm.

Image analysis

Confocal image data were analyzed using Volocity 3.6.1 and 4 (Improvision) or ImageJ software. Z-stack projections were obtained by using the z-projection function of LSM-5 software (Zeiss). Z-stack movies were obtained by exporting confocal stack slices as TIFF series and generating z-stack movies using QuickTime Player (Apple).

Measurement of cell dimensions

Marginal boarder length of 10–15 adjacent marginal EVL cells was determined by measuring the cell length of the vegetal margin rim between two cell contacts of one single cell with Image-J software. Cell lengths of 15 (30% epiboly) or 10 adjacent cells (50%–90%) from one embryo were summarized. Data for several embryos per stage were averaged and the standard error (SE) was determined. Measurement of the length to width ratio was performed as described (Koeppen et al., 2006).

3D representation of EVL lamellipodia

Z-stack projections of EVL stacks were generated using the "depth coding" application of the LSM5 software (Zeiss). The relative area of the flattened lamellipodia in the z-projections was determined using Volocity 3.6.1. software: the lamellipodia appearing in one complete image frame of a z-projection of an animal pole view of the gastrula were outlined manually. The outlined areas were then determined using the measurement tool. The measured relative lamellipodia area per image frame was determined for several embryos in each experiment and the average value calculated.

Statistical analysis

Student's t-test (Microsoft Excel) with two-tailed distribution was performed to evaluate the significance. Error bars correspond to standard error (SE) or standard deviation (SD). In several cases, calculated results were normalized to WT (set as 100%).

Results

Live epiboly phenotype

We performed a detailed analysis of live development of MZ*spg*^{m793} zebrafish embryos during epiboly to obtain a better understanding of the cellular changes that cause the abnormal epiboly phenotype previously reported (Lunde et al., 2004; Reim and Brand, 2006). Analysis of the live phenotype revealed specific differences between wild-type and MZ*spg*^{m793} embryos during early, mid, and late epiboly (Fig. 1).

At 1000 cell and high stage, shortly after midblastula transition, cell motility starts (Kane and Kimmel, 1993). At this stage, MZ*spg*^{m793} embryos displayed an enhanced constriction at the blastoderm-YSL interface (Figs. 1A, B). The average *o*uter *d*iameter (OD; equatorial extend of the YSL cytoplasmic margin at the interface between YSL and yolk mass) in MZ*spg*^{m793} embryos was about 8% smaller than that of age-matched wild-type embryos, and the average *i*nner *d*iameter (ID; interface between YSL and blastoderm) about 14% smaller. The overall size of wild-type and MZ*spg*^{m793} oocytes and embryos is not significantly different (Fig. S1).

As previously published (Lunde et al., 2004; Reim and Brand, 2006), MZ*spg*^{m793} embryos displayed a delay in the vegetal progression of epiboly (Figs. 1C–R) and an abnormal behavior of internalized cells (Figs. 1I–R). While the blastoderm in wild-type embryos started spreading over the yolk cell, the mutant blastoderm showed no epiboly progression (Figs. 1E–H), but developed translucent areas at the blastoderm to yolk cell margin (Fig. 1H, arrow). When age-matched wild-type embryos reached germ ring stage, only 30% epiboly progression was detectable in MZ*spg*^{m793} embryos (Figs. 1I, J). At a stage when wild-type control embryos have reached the end of epiboly, the deep cells of MZ*spg*^{m793} did not pass beyond 50% epiboly, and the EVL cells have reached only about 75–80% epiboly (Figs. 1Q, R). Thus epiboly of both EVL and deep cells appeared strongly retarded in MZ*spg*^{m793}. In the final phase of epiboly, a widening gap between the vegetal margin of the EVL and deep cells formed in MZ*spg*^{m793} embryos (Figs. 1M–N, arrowheads marking the respective margins of deep cells and EVL) and distortions in the YCL were detectable (Figs. 1P, P′, arrows), which appeared to displace the YCL and bring yolk mass and yolk cell membrane into close contact. The directed anterior migration of hypoblast cells toward the animal pole appeared to be not affected in MZ*spg*^{m793} embryos (Figs. 1N, P, R; arrow marking the leading edge of the anterior mesendoderm). At 60% epiboly stage of wild-type embryos, MZ*spg*^{m793} embryos displayed a small malformed shield (Fig. 1N′, asterisk, animal view). At the end of gastrulation, the animal view showed that the anterior hypoblast cells of *pou5f1*

deficient MZ*spg*^{m793} embryos have formed a polster like structure (Fig. 1R′).

Epiboly progression defects of the deep cells and EVL

To analyze the degree of epiboly delay in more detail, we stained nuclei to visualize the distribution of cells, and thus epiboly progression of deep cell and EVL compartments. Sytox green nuclear staining of fixed embryos confirmed the observed deep cell delay and revealed a severe EVL delay (Figs. 2B, D). In MZ*spg*^{m793} embryos, the mean distance between opposed deep cell layer margins was about 2.5 times broader than in age-matched 90% epiboly wild-type embryos. The mean distance of opposed EVL margins was about 3.4 times that of wild-type embryos. Analysis at about 95% epiboly identified an EVL delay also for MZ*spg*^{hi349} embryos (Figs. S2A–D), the other well characterized strong *spg* allele. Comparison of the two alleles showed that the average distance of opposed EVL margins was in the case of MZ*spg*^{hi349} 2 times, and in the case of MZ*spg*^{m793} embryos about 2.7 times broader than in wild-type embryos (Fig. S2D). Note that M*spg*^{m793}, in comparison to MZ*spg*^{m793}, displays much less affected deep cell migration, but still shows a retardation of epiboly (Fig. S3). Progression of the vegetal closure process, which easily detects epiboly delay in MZ and M*spg*^{m793}, revealed no significant difference between wild-type and Z*spg*^{m793} embryos (Fig. S4).

Delay of deep cell epiboly could be caused by abnormal migratory or adhesive behavior, but could also be caused by reduced number of deep cells, which therefore may not be able to properly spread over the yolk cell. We determined the number of cell nuclei in wild-type and MZ*spg*^{m793} embryos at exactly 4 hpf, when wild-type embryos have about 4000 cells, and at 5 hpf, when wild-type embryos have 8000 cells (Kimmel et al., 1995). The number of nuclei was determined for Sytox Green stained fixed embryos from confocal image stacks using automated object identification and measurement software (Fig. S4). Our data reveal that MZ*spg*^{m793} embryos have about 4000 nuclei, and thus cells, at 4 hpf, and 8000 nuclei at 5 hpf. Therefore synchronous pre-MBT and semi-synchronous post-MBT cell division cycles proceed at the same rate in wild-type and MZ*spg*^{m793} at least until cell division cycle 13. Wild-type embryos reach shield to 60% epiboly stage before the less synchronous cell division cycle 14 starts. This demonstrates that the delay in epiboly, at least until 50–60% epiboly stages, is not caused by reduced deep cell number.

In conclusion, we demonstrate that the epiboly delay of MZ*spg*^{m793} is constituted by a delay of both deep cells and EVL. In contrast to previous reports (Reim and Brand, 2006), we find that epiboly of the EVL is also delayed in MZ*spg*^{hi349} embryos, though slightly less severe when compared to MZ*spg*^{m793}. Thus both *spg*^{hi349} and *spg*^{m793} appear to act as functional null alleles with respect to epiboly movement, and the potentially truncated protein in *spg*^{m793} does not seem to act as a hypomorph. M*spg*^{m793} embryos lacking solely the maternal *pou5f1* contribution still showed a mild deep cell delay in epiboly progression, indicating that both maternal and zygotic *pou5f1* expression are required to control epiboly.

Distorted yolk cortical cytoplasmic layer integrity

To address cytoskeletal organization of the cortical layer, we performed anti-β-Tubulin immunohistochemistry of microtubules and Alexa488-Phallodin stainings of deposited F-Actin. Anti-β-Tubulin immunohistochemistry revealed a normal cortical microtubule network formation in MZ*spg*^{m793} embryos during cleavage and blastula stages (data not shown). However, most MZ*spg*^{m793} embryos develop a severely abnormal microtubule organization during epiboly progression (Figs. 3A–D, B′, D′). During the late phase of epiboly (starting at 50% epiboly) in wild-type embryos, a dense array of microtubules extends over the yolk cell. In MZ*spg*^{m793} embryos, large patches of the cortical cytoplasmic layer appeared to be devoid of microtubules, while some broad microtubule bundles extended over the yolk to the vegetal pole (Figs. 3D, D′). Analysis of Actin filament distribution (Figs. 3E, F, F′) revealed similar patches within the cortical cytoplasmic layer devoid of Actin filaments. Phenotypic comparison and statistical analysis indicated that this phenotype of the cortical cytoplasmic layer likely correlates with areas in live embryos where the yolk mass appeared to have displaced the cortical cytoplasm and thus gets in close contact with the yolk cell membrane (Figs. 1P, P′ and Fig. 3F″; Table 1). Western blot analysis of the total β-Tubulin protein amount revealed no difference between wild-type and MZ*spg*^{m793} embryos (data not shown). Analysis of M*spg*^{m793} embryos revealed no Tubulin or Actin free areas of the cortical layer as seen in MZ*spg*^{m793} embryos. In severe cases, the cortical cytoplasmic layer appeared non-homogeneous, with areas of less cortical elements (Fig. S6). Thus maternal Pou5f1 is required to control the proper cytoskeleton formation of the cortical layer, and zygotic expression of *pou5f1* can only partially rescue the mutant phenotype caused by the absence of maternal *pou5f1*.

Combined Hoechst33342 nuclear staining and anti β-Tubulin immunohistochemistry revealed abundant small spherical structures located within the cortical layer of MZ*spg*^{m793}, which are only rarely detected in wild-type embryos. Based on the fact that Hoechst33342 does not stain these vesicles (Fig. 3B′b, black arrow), they do not appear to be nuclei (Fig. 3B′b, white arrow), but vesicles surrounded by microtubules (Fig. S7). These spherical structures can also be visualized in live embryos using differential interference contrast optics (Figs. 3B″a, b, D″a, b). Furthermore, the microtubule stain also visualizes the location of dorsal forerunner cells (DFC). DFCs are a population of dorsal DEL cells which migrate ahead of the DEL margin and will later line Kupffer's vesicle (Cooper and D'Amico, 1996). Interestingly, in MZ*spg*^{m793} embryos, forerunner cells progressed independently of DEL velocity at a pace similar to the EVL (Figs. S8B, arrow, B′).

Delay of coordinated epithelial cell shape changes of marginal EVL cells

Recently it was shown that contractile elements are required for the constriction of marginal EVL cells, and thus for establishment of a purse-string mechanism that contributes to

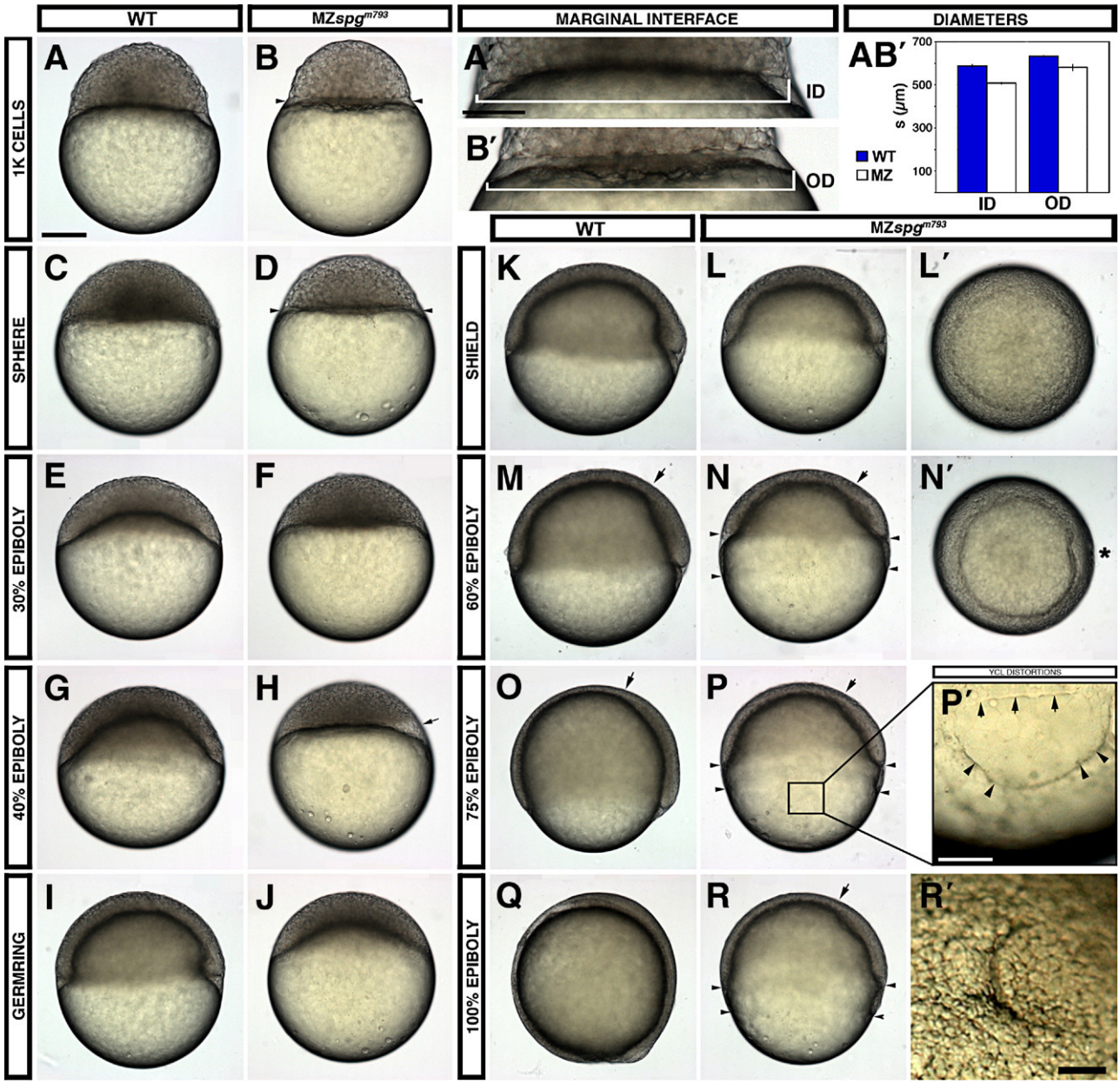

Fig. 1. Live phenotype of MZ*spg* embryos reveals severe gastrulation defects. (A–D) At the onset of cell motility, MZ*spg*^{m793} embryos display a smaller blastoderm with an enhanced constriction between DEL/EVL and YSL and an enlarged YSL (small arrowheads). (A′, B′) Higher magnification of the outer (interface between DEL and YSL) and inner (interface between YSL and YCL) diameter of WT versus MZ*spg*^{m793}. (A, B′) Measurements of the diameters including SE. *I*nner *d*iameter (ID): MZ*spg*^{m793}: 508±2 µm, WT: 587±4 µm; $p=4\cdot10^{-10}$. *O*uter *d*iameter (OD): MZ*spg*^{m793}=576±7 µm, WT=635± 2 µm; $p=1\cdot10^{-05}$. (E–H) While the blastoderm in WT starts spreading over the yolk, mutant blastoderm sits on the yolk cell showing translucent deep cell areas (H, arrow). (I, J) A 30% epiboly progress can be detected in MZ*spg*^{m793} when WT reach *germ ring* stage. (M, N, N′) At 60% epiboly mutant embryos display a widening gap (arrowheads) between EVL and DEL margin and a small malformed shield (N′, animal view, *). (N, P, R) Vegetally migrating deep cells and anteriorly migrating hypoblast cells in mutant embryos show retardation (arrow marking the leading edge of the anterior mesendoderm). (P′) Higher magnification of the mutant YCL showing cortical clefts (arrowheads); arrows indicate EVL margin. (Q, R) At the end of epiboly, the DEL as well as the EVL appears strongly retarded in MZ*spg*^{m793}. EVL cells seem to have reached about 75–80% epiboly, while deep cells seem not to have passed 50% epiboly. (R′) Animal view of mutant embryos shows a polster like formation. Staging of live embryos has been repeated in three independent experiments with equal results. Embryos were synchronized at the four cell stage. Scale bars: overview pictures: 300 µm; higher magnification: 100 µm.

epiboly progression during the late phase of epiboly (Cheng et al., 2004; Koeppen et al., 2006). To address the establishment of F-Actin rings and integrity of the punctuate Actin band, we stained embryos with Alexa488-Phalloidin. Z-projections of stained embryos revealed a delay of the constriction of marginal EVL cells in MZ*spg*^{m793}, showing rounder marginal EVL cells resulting in a longer marginal cell length at the border of the EVL margin to the YSL (Figs. 4A–F).

To compare quantitatively the differences in marginal cell constriction between wild-type and MZ*spg*^{m793} embryos, the length of the vegetal margin of individual border cells for 10 to 15 cells per embryo was measured. These values of the

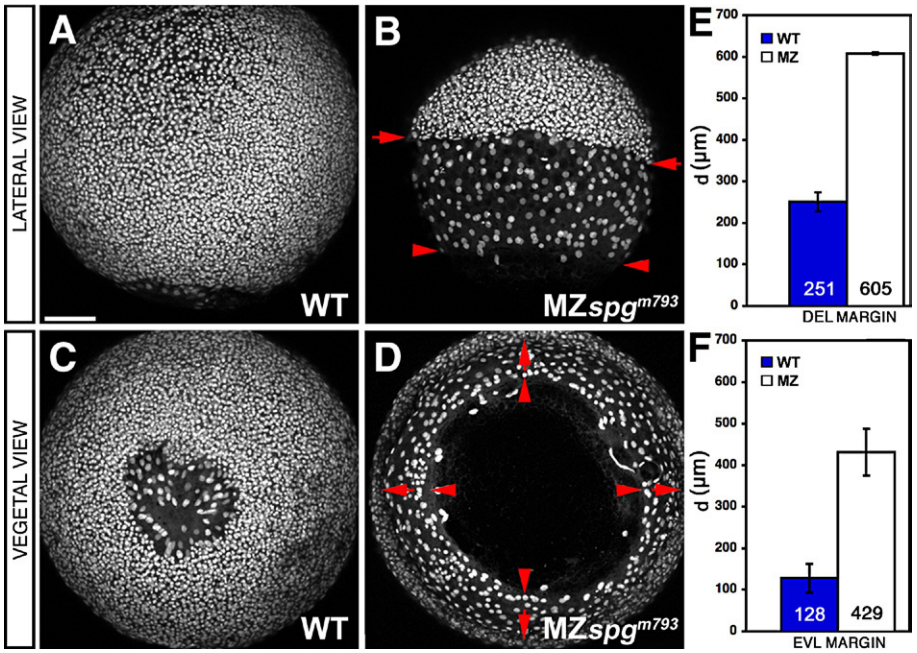

Fig. 2. Epiboly delay of the DEL and EVL. (A–D) Confocal z-projections of Sytox green stained embryos at 85% epiboly stage. MZ*spg*^{m739} embryos show a strong DEL (arrows) and EVL (arrowheads) retardation. (A, B) Lateral and (C, D) vegetal views. (E) Measurements of the mean diameter "d" of diametral DEL margins: WT=251±26 µm, MZ*spg*^{m793}=605±6 µm, $p=2\cdot10^{-08}$. (F) Measurements of the mean diameter "d" of diametral EVL margins: WT=128±31 µm, MZ*spg*^{m739}=429±13 µm ($p=1\cdot10^{-06}$). Scale bar: 100 µm.

averaged marginal cell border length were determined for several embryos, and averages, SE, and *p*-values calculated (embryo numbers are indicated in the graphs; Fig. 4G). The results were then normalized on wild-type values (100%). MZ*spg*^{m793} embryos had a significantly longer marginal cell border length compared to wild-type at 50% epiboly and shield stage (Fig. 4G). The more rounded MZ*spg*^{m793} marginal cells can clearly be distinguished from wild-type. Note that at later stages from 75% to 90% epiboly, the state of constriction appeared to be inadequately described by marginal cell border length, as border cells progressively flatten. Analysis of M*spg*^{m793} embryos revealed that a delay in the coordinated epithelial cell shape changes of the EVL is also apparent in embryos lacking the maternal *pou5f1* expression (Fig. S3). Another measure for the changes in EVL cell shape is the length to width ratio of marginal cells. We measured and compared length to width ratios of MZ*spg*^{m793} embryos and wild-type at 50%, 75%, and 90% epiboly (Fig 4H). No significant differences in cell shape can be detected by this ratio at 50% epiboly. While at 75% the average ratio indicates that MZ*spg*^{m793} cells are still rounder than wild-type cells, this change is not statistically significant (Student's *t*-test). However, at 90% epiboly MZ*spg*^{m793} cells have a significantly less elongated cell morphology compared to wild-type ($p<0.05$).

While the marginal purse-string mechanism may contribute to late epiboly, vesicle trafficking at the YSL, vegetal to the EVL margin had been suggested to contribute already to early phases of epiboly (Betchaku and Trinkaus, 1978; Betchaku and Trinkaus, 1986; Solnica-Krezel et al., 1995). We analyzed the existence of endocytic vesicles at the marginal rim vegetal to the EVL margin following Lucifer Yellow incubation, and found no differences between MZ*spg*^{m793} and wild-type (Fig. S9).

Lamellipodia phenotype of the EVL

To investigate the integrity of the EVL cells in more detail, we performed confocal analysis of the animal pole of Alexa488-Phalloidin stained embryos. High magnification confocal z-stacks revealed an abnormally high degree of EVL cell lamellipodia formation during the late phase of epiboly in MZ*spg*^{m793} embryos (Figs. 5A–F). While the deep cell shapes appeared not to be different from age-matched wild-type embryos (Fig. S10), the EVL cells of MZ*spg*^{m793} embryos showed significantly more lamellipodia formation for the analyzed stages 75% and 90% epiboly, giving a ruffled appearance to the cell borders. In contrast, at 60% epiboly, no significant differences were detected (Fig. 5G). Analysis at 90% epiboly stage also revealed extensive lamellipodia formation for MZ*spg*^{hi349} embryos (Figs. S11B, E). MZ*spg* embryos rescued by early injection of *pou5f1* mRNA showed a wild-type like non-lamellipodia phenotype of the EVL, which confirms this phenotype being associated with the loss of *pou5f1* in MZ*spg* embryos (Fig. S11F).

Non-cell autonomous phenotype of MZspg^{m793} *deep cell migration*

To address if the deep cell delay in MZ*spg* is mainly due to cell intrinsic or to extrinsic alterations, we performed co-transplantation experiments of mixed wild-type and MZ*spg*^{m793}

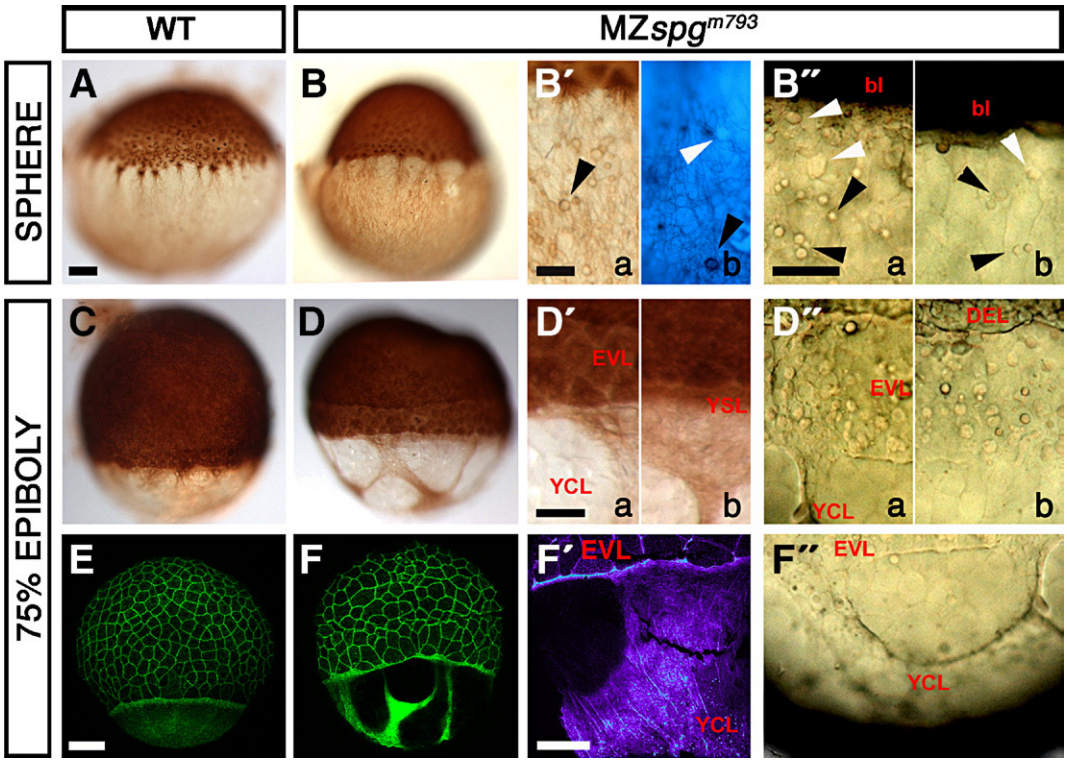

Fig. 3. Distorted yolk cell cortical layer integrity. (A–D, B′, D′) Anti-β-Tubulin/DAB staining of the cortical Tubulin network in MZ*spg*^{m793} and WT embryos, as indicated. (B′b) Combined Höchst33342/anti-β-Tubulin-antibody/DAB stainings of MZ*spg*^{m793} embryos showing small spheres (arrowheads) located within the cortical layer of non-nuclear origin. (B″) Small cortical spheres (arrowheads) in a living MZ*spg*^{m793} embryo. (C, D) Shield stage. (D) Formation of a gap between DEL and EVL in MZ*spg*^{m793} embryos. (D, D′) Anti-Tubulin stained embryos reveal cortical layer distortions with areas that appear devoid of a cytoplasmic layer. (D″, F″) Cortical layer distortions in living MZ*spg*^{m793} embryos (arrowhead). (E, F) Confocal z-projections of Alexa488-Phalloidin stained embryos visualize Actin filament distribution. (F) Distortions of the punctuate band and the continuous Actin deposition in the YCL in MZ*spg*^{m793} embryos. (F′) Color depth-coded projection of confocal image stack. Subpanels in panels B′, B″, D′, and D″: (a) strong, (b) mild phenotypes. bl: blastoderm, EVL: enveloping layer, DEL: deep cell layer, YCL: yolk cytoplasmic layer, YSL: yolk syncytial layer. Scale bar: 100 μm.

cells into wild-type or mutant hosts. This makes it possible to assay cell motility differences in genetically homogenous environments. Cell velocity was determined from confocal time lapse images followed by manual tracking of individual cells at ventral positions (Fig. 6, Movies S1 and S2). The net velocity of MZ*spg*^{m793} cells in a wild-type environment corresponded to 95±13% of the wild-type velocity, which was set as 100% (p=0.828). The net velocity of MZ*spg*^{m793} cells in MZ*spg* environment corresponded to 110±18% (p=0.824) of the wild-type net velocity. Detailed comparison of deep cell net velocity therefore revealed no significant difference between wild-type and MZ*spg*^{m793} cells (Figs. 6C, F).

Table 1
Classification of defects in the yolk cell cortical layer

	Genotype	Sphere			50% epiboly			75% epiboly		
		Class I	Class II	n	Class I	Class II	n	Class I	Class II	n
Tubulin network	WT	24	0	3	12	1	2	6	0	2
	MZ*spg*^{m793}	18	0	2	8	23	2	5	23	2
Actin network	WT	–	–	–	16	0	3	12	4	4
	MZ*spg*^{m793}	–	–	–	11	2	2	2	25	4

Embryos were stained for microtubules or F-Actin as in Fig. 3. Embryos were classified based on phenotype into: Class I embryos have a wild-type like structure with continuous cortical layer; and Class II a distorted cortical layer with cytoskeletal defects resembling a severe phenotype of MZ*spg*^{m793}. The number of independent experiments combined to assemble data is indicated by n.

Our velocity measurements confirmed previous predictions that altered extrinsic factors seem to result in the abnormal epiboly behavior of *pou5f1* deficient cells (Reim and Brand, 2006). Such non-cell autonomous mechanisms could include differences in protrusive activity, cell adhesion, or long range cues. Our transplantation assays indicate that MZ*spg*^{m793} cells can read the directionality provided by potential long range cues—if such cues exist at all for influencing epiboly movements.

Behavior of cells at the ventral margin

To obtain more insight into the epiboly migration behavior of cells, we performed live confocal time lapse recordings of cells with fluorescently marked membranes (membrane tagged GFP) and nuclei (Sytox green). To minimize interference of convergent extension movements with our measurements, we chose cells at the ventral leading edge (Figs. 7A, B). We observed in MZ*spg*^{m793} embryos that deep cells attempt to fill the developing gap between EVL and YSL until about 40 min post shield stage (about 75% epiboly), but fail as epiboly

progresses. This results in the formation of a large cavity between EVL and YSL, into which deep cells do not enter (Fig. 7B; Movie S5).

We further analyzed EVL cell behavior at the blastoderm margin in wild-type embryos (Figs. 7C, D). Higher magnification showed that EVL cells are not only tightly attached to the YSL (Koeppen et al., 2006), but also establish filopodia at the interface between EVL and YSL protruding toward the site of migration in a manner as to sense the environment for guidance cues. Filopodia could be detected at the EVL leading edge of wild-type (Fig. 7C, red arrow, Movies S3 and S4) and of time-matched MZ*spg*^{m793} embryos (Movie S5). The deep cells, EVL, and YSL showed intensive protrusive activity between all three layers during epiboly. Higher magnification depicted wild-type deep cells projecting filopodia toward the EVL (Fig. 7D, white arrowhead, Movie S4) supporting the hypothesis that the EVL serves as a migration substrate for deep cells (Shimizu et al., 2005). EVL defects may negatively influence deep cell migration (Shimizu et al., 2005). The analysis of the live phenotype and of the cytoskeleton in *pou5f1* deficient embryos revealed distortions of the yolk cortical cytoplasmic layer. As the EVL is tightly attached to the YSL/YCL (Koeppen et al., 2006), the epiboly progression defect of the YSL/YCL may thus initiate a chain of events causing EVL and indirectly deep cell delay.

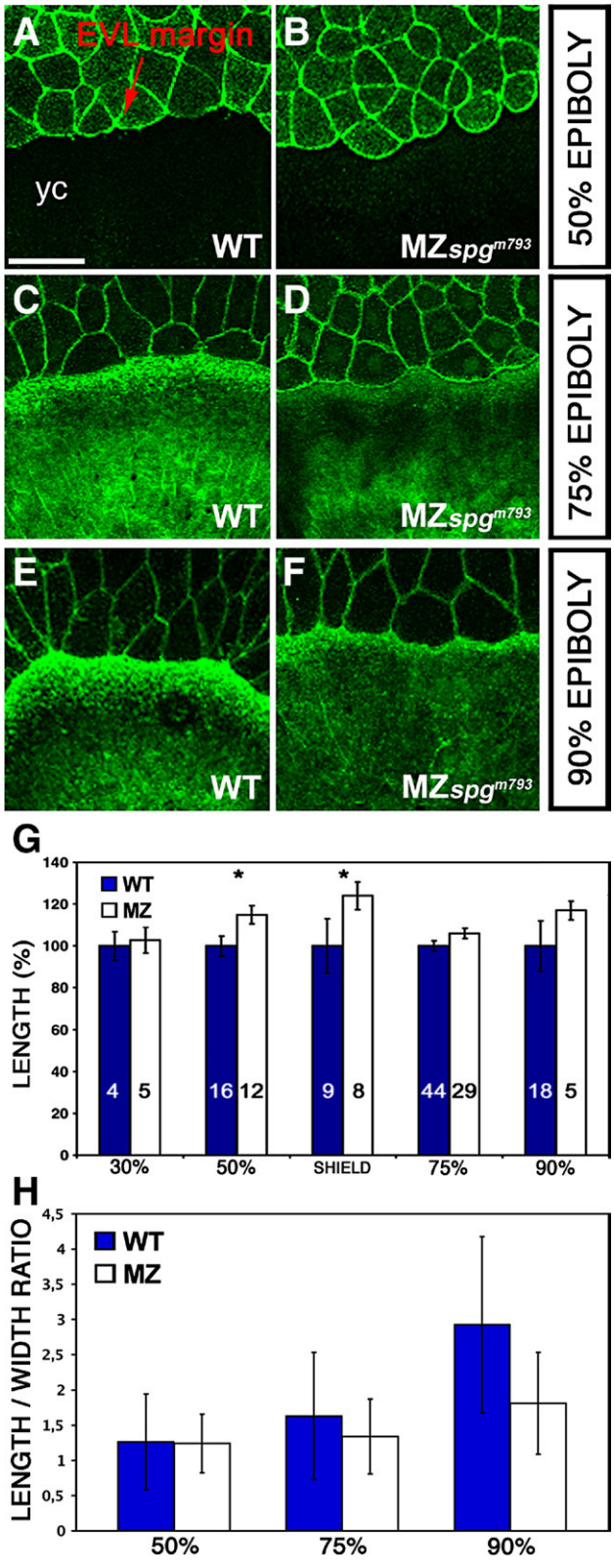

Fig. 4. Delay in cell shape changes of marginal EVL cells. (A–F) Confocal z-projections of Alexa488-Phalloidin stained embryos showing a delay in flattening of marginal EVL cells. (A, C, E) WT; (B, D, F) MZ*spg*^{m793} embryos. (A, B) 50% epiboly; (C, D) 75% epiboly; (E, F) 90% epiboly. All MZ*spg*^{m793} stages are time-matched to wild-type embryos. yc: yolk cell. Scale bar: 100 µm. (G) Measurements of the average border cell length of 10–15 marginal EVL cells including SE. 30% epiboly: WT=100±8%; MZ*spg*^{m793}=103±6% (p=0.205). 50% epiboly: WT=100±5%; MZ*spg*^{m793}=115±4% (p=0.029). Shield stage: WT=100±4%; MZ*spg*^{m793}=124±7% (p=0.011). 75% epiboly: WT=100±2%; MZ*spg*^{m793}=246±2% (p=0.069). 90% epiboly: WT=100±12%; MZ*spg*^{m793}=117±5 (p=0.122). Data were normalized on WT results set as 100%. Asterisks highlight significant differences. (H) Measurements of the length to width ratio of marginal EVL cells. For each stage the length to width ratio of 10 adjacent cells was determined in 10 embryos of each wild-type or MZ*spg*^{m793}. The graph represents average data from 100 cells for each genotype and stage, bars indicate standard deviation. 50% epiboly: MZ*spg*^{m793}=1.24±0.42; WT=1.26±0.68 (p=0.8004; paired Student's t-Test); 75% epiboly: MZ*spg*^{m793}: 1.34±0.53; WT=1.63±0.90 (p=0.2349); 90% epiboly: MZ*spg*^{m793}=1.81±0.72; WT=2.93±1.25 (p=0.0000000615). Number of analyzed embryos is depicted within bars.

Altered cell adhesion properties of pou5f1 deficient cells

The adhesiveness of wild-type and *pou5f1* deficient cells was compared by utilizing the sorting out mechanism of cells with different adhesive properties in an *in vitro* cell culture approach (Davis et al., 1997; Montero et al., 2003; von der Hardt et al., 2007). Primary co-cultures of dissociated sphere stage wild-type and MZ*spg*^{m793} embryos were generated from embryos injected either with Rhodamine-dextran or Alexa488-dextran, respectively. Color labeled dissociated cells were mixed and plated on Fibronectin/Collagen coated dishes. The dissociation was verified by confocal imaging shortly (within 15 min) after plating, and the aggregation of the cells was monitored after 4 and 16 h.

Shortly after dissociation, differently labeled cell types efficiently mixed (Figs. 8A–C). After 4 h of incubation, formation of intermingled clusters appeared (Figs. 8D–F). After

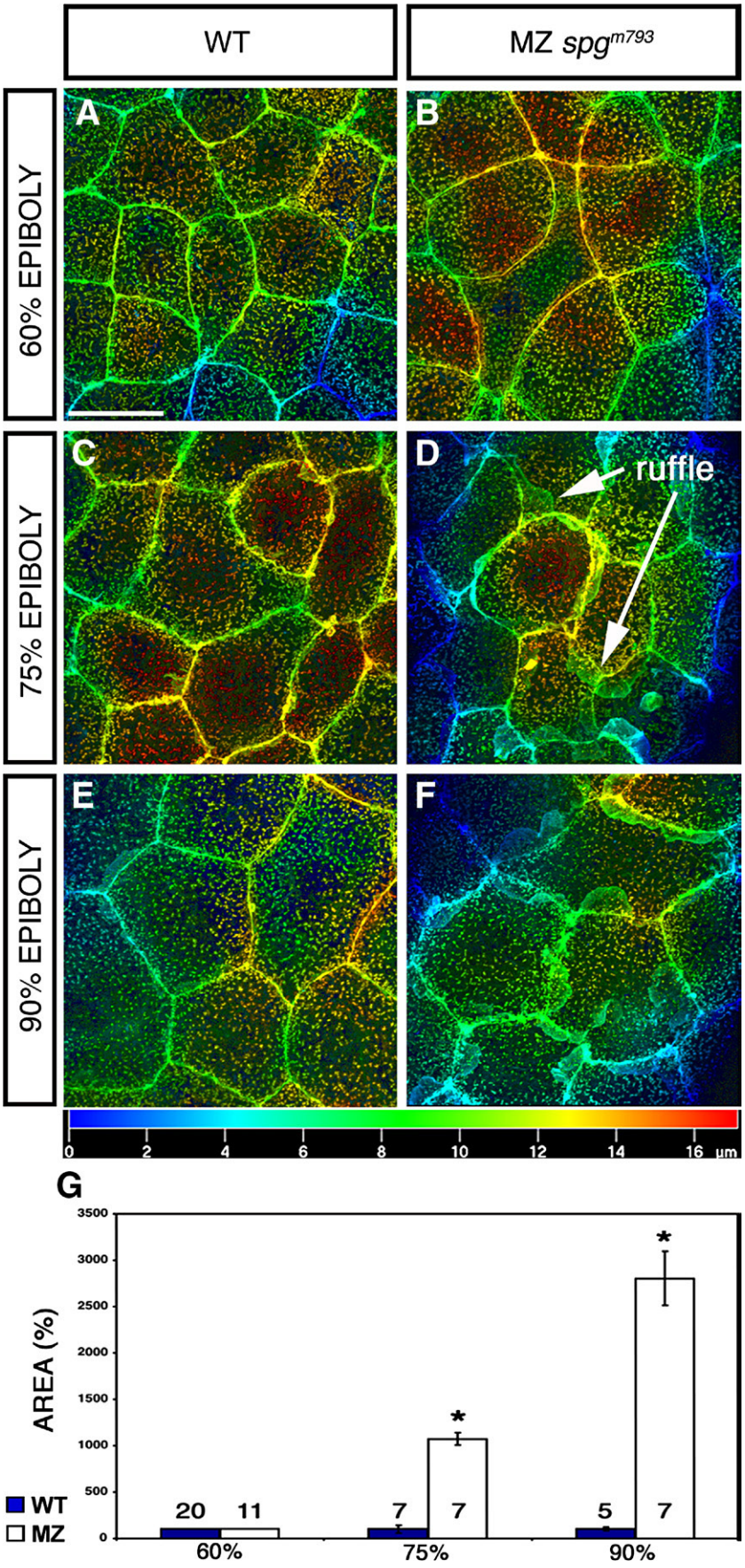
WT
MZ spg^m793
60% EPIBOLY
75% EPIBOLY
90% EPIBOLY
A
B
C
D
ruffle
E
F
0 2 4 6 8 10 12 14 16 µm
G
AREA (%)
3500
3000
2500
2000
1500
1000
500
0
WT
MZ
20 11
7 7
5 7
*
*
60%
75%
90%

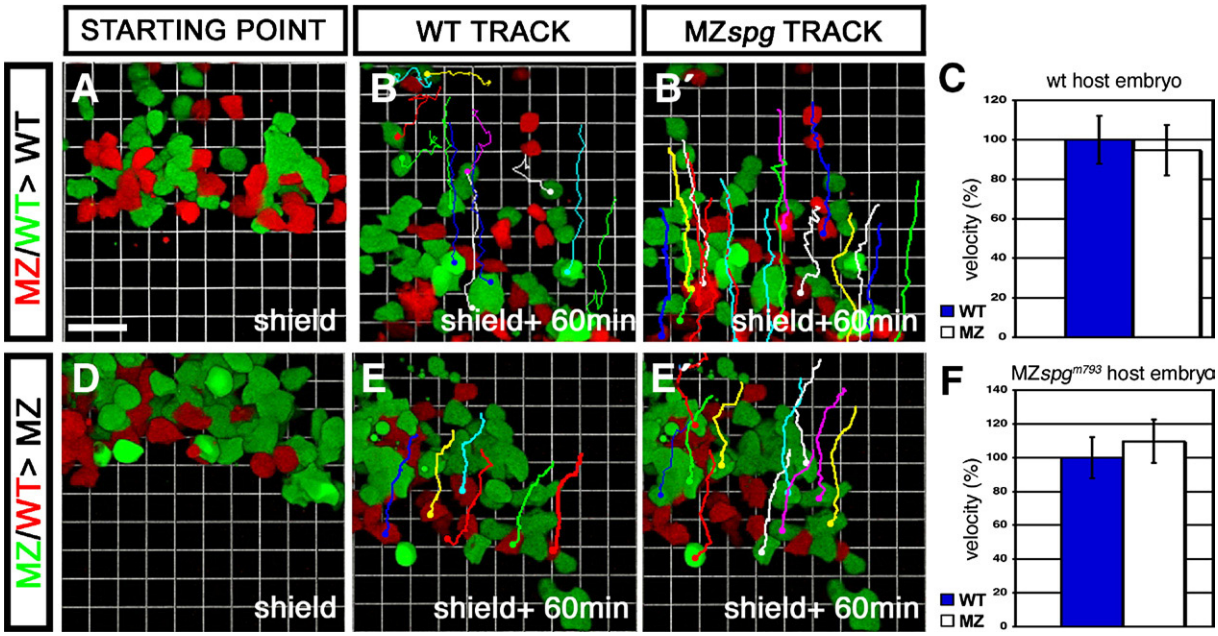

Fig. 6. Non-cell autonomous delay of DEL cell migration in MZ*spg* embryos. Confocal z-stack time lapse recordings of mosaic embryos, starting at shield stage for 60 min. An approximately equal amount of cells from WT and MZ*spg*^{m793} donors labeled with different fluorescent dyes were collected and co-transplanted into the ventral margin of a non-labeled host. Donors were either labeled with Alexa488-dextran (MW: 10 kDa) or Alexa546-dextran (MW: 10 kDa). (A, B) Cells transplanted into a WT host. (D, E) Cells transplanted into a MZ*spg*^{m793} host. (B, E) Tracking lines of transplanted WT cells. (B′, E′) Tracking lines of transplanted MZ*spg*^{m793} cells at the end of the time lapse. (C, F) Measurements of the net velocity of 10–20 transplanted cells. Velocity was normalized on WT velocity and depicted as % of WT data including standard deviation. (C) Net velocity of cells in a WT environment ($n=4$): WT = 100 ± 12%; MZ*spg*^{m793} = 95 ± 13%; $p=0.828$. (F) Net velocity of cells in a *pou5f1* deficient environment ($n=2$): WT = 100 ± 22%; MZ*spg*^{m793} = 110 ± 18%; $p=0.825$. No significant difference in velocity was observed. Scale bar: 46.2 µm (see also Movies S1 and S2).

16 h of incubation, cells of different genotypes in mixed cultures of MZ*spg*^{m793} and wild-type cells were observed to have sorted out into distinct subclusters (Figs. 8H, I, M, K, L), and only 1.5 ± 0.7% of all analyzed heterogeneous clusters appeared to be intermingled. Genetically homogeneous WT–WT co-cultures showed predominantly intermingled clusters (97 ± 0%; Figs. 8G, J, M). Thus genetically homogeneous and heterogeneous clusters displayed a significant difference in their aggregation behavior (p-value < 0.004; Fig. 8M).

To further evaluate adhesiveness of the different cell types, we analyzed subcluster size and cluster organization. In genetically heterogeneous clusters, the predominant cell genotype was wild-type in 73 ± 12.5% of all analyzed clusters. Only 13.2 ± 2.5% MZ*spg*^{m793} cells made up the main portion. An equal cell genotype contribution appeared in 12.2 ± 9.8% of all clusters (Fig. 8N). Note that in this classification the different cell genotypes were not intermingled but located in distinct subcluster areas (Figs. 8K, L). In conclusion, these data revealed that *pou5f1* deficient cells and wild-type cells have different adhesive properties.

Discussion

Pou5f1/Oct4 is mainly regarded as a stem cell factor contributing to self-renewal of stem cells and pluripotency (Ovitt and Scholer, 1998; Pesce et al., 1998; Pesce and Scholer, 2001; Pan et al., 2002; Takahashi and Yamanaka, 2006). However, in the vertebrate embryo, the cells that express Pou5f1, besides being pluripotent, also have a characteristic cellular behavior typical for this stage of embryogenesis, which may be blastula to early gastrula stages in lower vertebrates like fish, or blastocyst to cylinder stages in mammals. This behavior includes spreading and reorganization, as well as migratory aspects, and specific cell adhesion (Solnica-Krezel, 2006). We utilized MZ*spg* zebrafish mutant embryos, which are devoid of Pou5f1 activity, to investigate the contribution of Pou5f1 to cellular behaviors during gastrulation. While the three lineages of the early zebrafish embryo, the extra-embryonic EVL and YSL, and the embryonic deep cell layer act in concert during gastrulation, we will discuss changes observed in *pou5f1* deficient MZ*spg* in each lineage separately first.

Fig. 5. Enhanced lamellipodia formation of EVL cells. Animal pole confocal z-projections of Alexa488-Phalloidin stained embryos during epiboly. (A–F) EVL cells. (A, C, E) WT EVL cells with few detectable lamellipodia. (B, D, F) MZ*spg*^{m793} EVL cells with enhanced lamellipodia formation at the cell–cell contact site of EVL cells, projecting toward the deep cells, (A, B) at 60% epiboly, (C, D) at 75% epiboly, and (E, F) at 90% epiboly. Images show z-projections of confocal stacks of images using the depth coding method, to visualize the localization of lamellipodia. Depth scale bar is depicted beneath panels E and F. Scale bar: 20 µm. (G) Measurements of the lamellipodia area including SE: 60% epiboly: WT = 100 ± 0%, MZ*spg*^{m793} = 100.75 ± 0% (no lamellipodia detectable). 75% epiboly: WT = 100 ± 40%; MZ*spg*^{m793} = 1072 ± 67% ($p = 3.157 \cdot 10^{-08}$). 90% epiboly: WT = 100 ± 20%; MZ*spg*^{m793} = 2804 ± 290% ($p = 2.563 \cdot 10^{-06}$). Measurements were performed with Volocity software. Data were normalized to WT results which was set as 100%. Asterisks highlight significant differences. Number of analyzed embryos is depicted within or above bars.

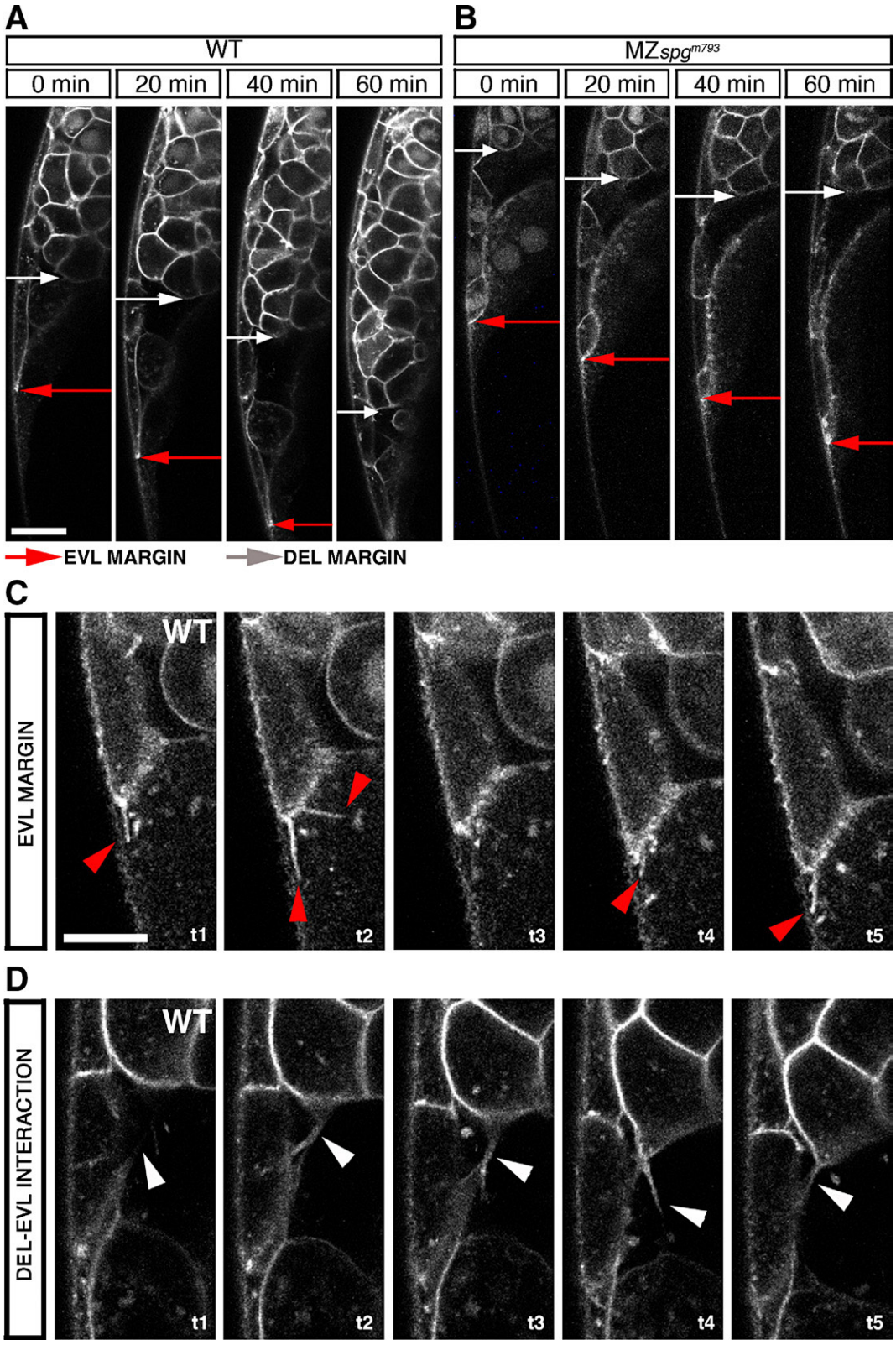

Fig. 7. Behavior of cells at the ventral margin. (A–D) Live phenotype observations of the ventral leading edge during a time course of 60 min. Membrane tagged GFP/Sytox green labeled embryos were monitored by confocal z-section time lapse analysis during a time course of 1 h starting at 60% epiboly stage. Red arrows mark the EVL leading edge, white arrows the DEL leading edge. (A) Shows the WT leading edge. (B) Shows the MZ*spg*^{m793} leading edge. (C) Filopodia formation at the interface between EVL and YSL in a WT embryo (red arrowheads). $\Delta t = 100$ s. (D) Filopodia formation between DEL, EVL in WT (white arrowheads). $\Delta t = 250$ s. (A, B) Scale bar: 100 μm. (C, D) Scale bar: 50 μm (see also Movies S3, S4, and S5).

Deep cell layer

Deep cells will constitute the embryo proper, and ubiquitously express *pou5f1* until internalization of marginal deep cells is initiated, and the hypoblast forms. After hypoblast formation, *pou5f1* expression is restricted to the epiblast, which will later form all ectodermal lineages (Takeda et al., 1994). The severe delay in deep cell epiboly is the most obvious phenotype, when observing early development of live MZ*spg* embryos (Lunde et al., 2004; Reim et al., 2004; Reim and Brand, 2006). It is already detectable from dome to 30% epiboly stage onwards, as doming of the yolk cells is less pronounced. One explanation why deep cells do not enter the space that opens during epiboly between EVL and yolk cell may be a potential reduction in deep cell number, in case the stem cell factor Pou5f1 would affect early proliferation in zebrafish. However, we have analyzed deep cell numbers up to 50% epiboly, and do not see a significant reduction in *pou5f1* deficient MZ*spg* embryos during the post MBT proliferation cycles 11, 12 and 13. Thus the deep cell epiboly delay is likely a defect in cell behavior and not due to a reduced cell number. A comparison of deep cell motility between wild-type and MZ*spg* cell groups co-transplanted into wild-type or *pou5f1* deficient hosts revealed no significant difference in their net velocity. These findings suggested that the deep cell delay of MZ*spg* embryos is controlled in a non-cell autonomous manner (Figs. 6C, F). Results from our cell tracking correspond to previous studies using two time point comparisons in a similar experiment (Reim and Brand, 2006). Thus the epiboly delay appears not to be caused by an intrinsic inability of *pou5f1* deficient cells to behave like wild-type cells—a finding also supported by a study of the protrusive cellular behavior (filopodia and lamellipodia activity) observed by *in vivo* time lapse recordings using DIC optics (data not shown) and 4D confocal acquisition (Fig. 7).

Cell co-culture experiments revealed differences in adhesiveness of dissociated *pou5f1* deficient deep cells and wild-type cells. Recently it was shown that BMP signaling controls the convergence migration of mesodermal cells by negatively regulating their Ca^{2+}-dependent adhesiveness in a non-cell autonomous manner (von der Hardt et al., 2007). Although MZ*spg* embryos are dorsalized and deficient in expression of the ventralizing *bmp2b*, *4*, and *7* genes (Reim and Brand, 2006), we do not think that loss of BMP activity is the main cause of the observed epiboly defects. First, canonical BMP/Alk8 signaling has been proposed to negatively regulate cell adhesiveness (Mintzer et al., 2001; von der Hardt et al., 2007), but our data do not point to enhanced adhesiveness in MZ*spg* embryos. Second, even strongly dorsalized embryos like *swirl* or MZ*alk8* embryos display a much less severe delay in epiboly (Mullins et al., 1996; Mintzer et al., 2001). Third, genetic analysis in zebrafish has revealed that all so far characterized zygotic mutations that display a severe delay of epiboly progression could recently be linked to the *cdh1* locus encoding the Ca^{2+}-dependent surface molecule E-Cadherin (Kane et al., 1996a, 2005; McFarland et al., 2005). The delay of the deep cell layer in *cdh1* deficient embryos is proposed to be due to an affected radial intercalation process caused by the loss of asymmetric E-Cadherin distribution (Kane et al., 1996b, 2005; McFarland et al., 2005; Shimizu et al., 2005). Interestingly, similar to MZ*spg* embryos, *cdh1* morphants display epiboly defects without showing cell autonomous migration defects, when cells are transplanted into *cdh1* morphant or wild-type environments (Shimizu et al., 2005). However, *cdh1* mRNA expression and western blot analysis of total E-Cadherin amounts in MZ*spg* embryos revealed no significant quantitative changes (data not shown; Reim and Brand, 2006). Morphological similarities suggest that defects in cell adhesiveness might be the cause for the abnormal deep cell epiboly progression in MZ*spg*. The non-cell autonomous effects on migration behavior in *pou5f1* deficient embryos may reflect changes in extracellular signals, or intrinsic changes that result in alterations of the extracellular matrix, and may thus influence the migration behavior (Goto et al., 2005; Wallingford, 2005).

Yolk cytoplasmic and syncytial layers (YCL/YSL)

The yolk cell has yet been shown to contribute to epiboly through three mechanisms:

(1) A ring of YSL endocytic vesicles may move membrane material from the vegetal side of the EVL margin to more animally located positions, to support YSL epiboly (Betchaku and Trinkaus, 1986). Our data show that the ring of endocytic vesicles forms in MZspg^{m793} (Fig. S9).
(2) Long microtubule arrays, extending in the cortical layer from nucleation asters in the YSL to the vegetal pole, have been shown to contribute in pulling the YSL with the tightly attached EVL vegetalwards (Strahle and Jesuthasan, 1993; Solnica-Krezel and Driever, 1994). Distortions of the cortical layer in MZ*spg* embryos were already visible in live embryos. Anti-β-Tubulin stainings revealed a variable but consistent microtubule defect for MZ*spg* embryos (Figs. 3A–D′; Table 1), showing large bundles of microtubules separated by patches devoid of microtubules. This phenotype resembles taxol treated embryos (Solnica-Krezel and Driever, 1994). Taxol is a microtubule binding molecule which stabilizes the microtubule structure and thus inhibits fast remodeling of the cytoskeleton. The small spheres we observed to be included within the cortical layer (Figs. 3B′, B″, black arrow; Fig. S7) may be small cargo vesicles delayed during transportation to the blastoderm. The phenotypic similarity between taxol treated embryos and MZ*spg* embryos suggests that expression of a protein influencing Tubulin network dynamics and acting within the cortical layer may be altered in *pou5f1* deficient MZ*spg* embryos. Expression of this activity appears to depend both on maternal and zygotic Pou5f1, as MZ*spg* embryos displayed a similar but less severe microtubule phenotype (Figs. S6A–E). Protein levels of β-Tubulin in *pou5f1* deficient and wild-type embryos are not altered (data not shown). Staining of the Actin cytoskeleton revealed that F-Actin is also excluded form the microtubule free patches (Fig. 3F).

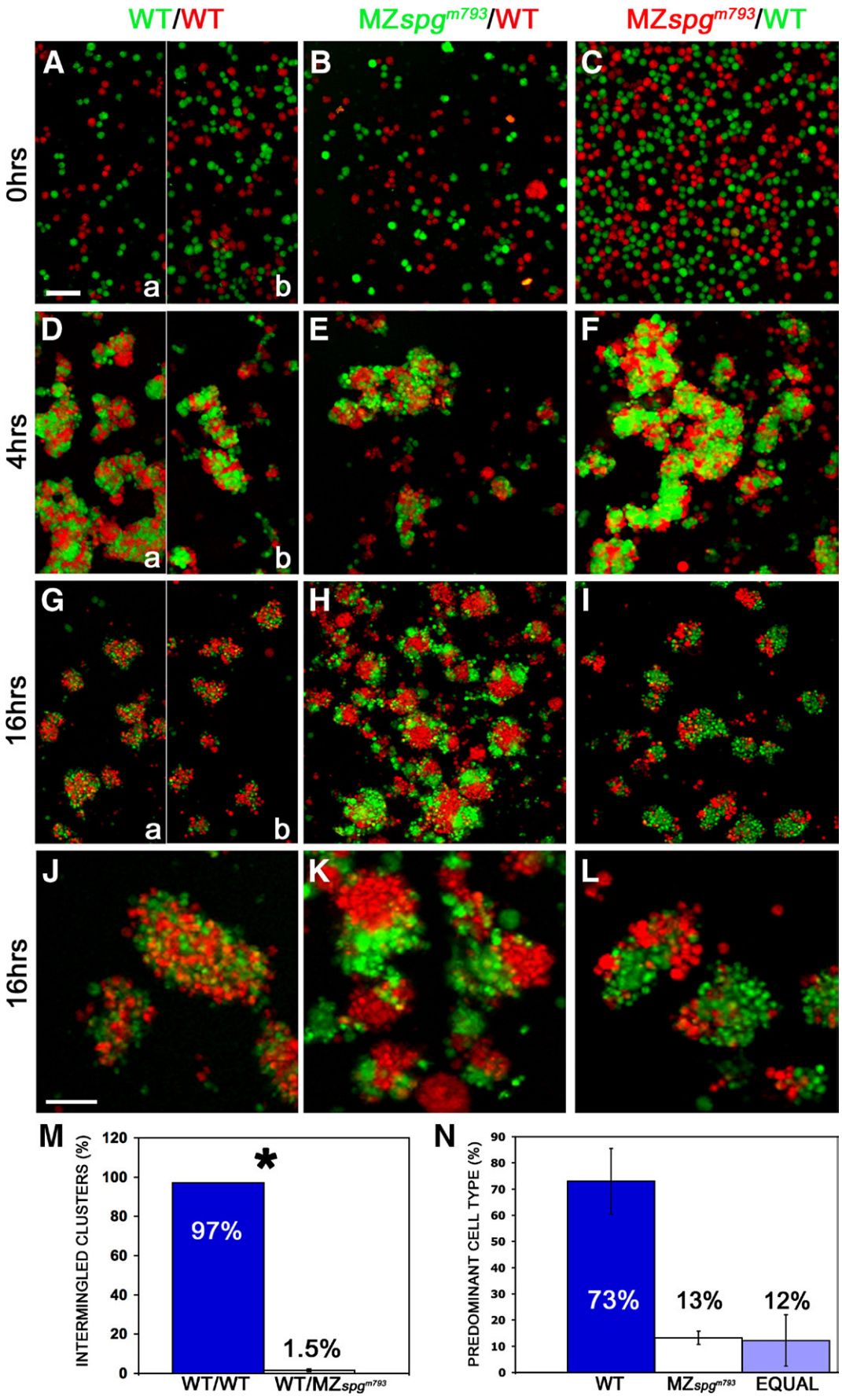
WT/WT
MZspg^m793/WT
MZspg^m793/WT
0hrs
4hrs
16hrs
16hrs
A
B
C
D
E
F
G
H
I
J
K
L
a
b
M
INTERMINGLED CLUSTERS (%)
120
100
80
60
40
20
0
*
97%
1.5%
WT/WT
WT/MZspg^m793
N
PREDOMINANT CELL TYPE (%)
90
80
70
60
50
40
30
20
10
0
73%
13%
12%
WT
MZspg^m793
EQUAL

(3) A ring of YSL F-Actin filaments forms after 50% epiboly at the vegetal margin (Cheng et al., 2004) and contributes to completion of epiboly, as inactivation of the formation of the contractile ring within the YSL specifically affects cell shape changes of the EVL required for completion of epiboly and yolk plug closure (Koeppen et al., 2006). While F-Actin can be detected in the punctuate band of the external YSL of MZ*spg* embryos, it appears to be less than in wild-type embryos (Fig. S2).

Enveloping layer (EVL)

A delay of EVL epiboly is difficult to detect, and in a previous study EVL epiboly was reported to be normal in MZ*spg*^{hi349} embryos (Reim and Brand, 2006). However, our analysis clearly documented an EVL retardation for MZ embryos of both strong *spg* alleles, *hi349* and *m793* (Fig. 2, Fig. S2). Recently it was shown that F-Actin rings in the vegetal EVL margin and the external YSL drive the late phase of epiboly (Cheng et al., 2004). Contractile elements located within the external YSL control the marginal constriction of EVL cells, and both appear to establish a purse-string mechanism that contributes to EVL epiboly (Koeppen et al., 2006). The finding that Actin and Myosin2 function within the YSL is required to effect EVL cell shape changes caused this mechanisms to be considered as coordinated epithelial cell shape change. The delay we observe in flattening of marginal MZ*spg* EVL cells may correlate with changes we observed in the F-Actin distribution in the external YSL (Fig. S3). A similar phenotype was reported for interference with the activity of the mitogen activated protein kinase kinase kinase kinase (MAP4K) Misshapen (Koeppen et al., 2006). Thus, Pou5f1 may control the transcription of genes required to control the contractile activity within the YSL.

The consistently enhanced lamellipodia formation of EVL cells in MZ*spg* embryos gives rise to ruffle like cell structures suggesting excessive Rac signaling. Enhanced lamellipodia formation, or failure of lamellipodia to adhere to the substrate may result in the formation of ruffles. Ruffle formation may indicate alterations of the EVL adhesive properties, but may also be due to alterations in extracellular matrix composition. Recently it was shown that cells of *angiomotin-like2* (*amotl2*) deficient zebrafish embryos display reduced protrusive activity, with ruffles nearly absent (Huang et al., 2007). *amotl2* is a gene required for formation and ordered array of Actin filaments during early embryogenesis. Amotl2 forms complexes with c-Src kinases and promotes their translocation from the perinuclear region to focal adhesion sites (Huang et al., 2007), and thus enhances their migratory properties. Candidates for the Src tyrosine phosphorylation that disrupt cadherin-dependent cell–cell contacts include ZO1 and ERM proteins (Ezrin/Moesin), which have been implicated in Cadherin–dependent adhesion strength (Owens et al., 2000, Takeda et al., 1995, Imamura et al., 1999) and coordinated epithelial cell shape changes (Koeppen et al., 2006). While the inverse phenotype (with respect to MZ*spg*) makes *amotl2* an unlikely direct target of Pou5f1 activity, Pou5f1 could control transcription of negative regulators of protrusive activity and the Rac pathway.

Here, we describe for the first time at the EVL–YSL interface an EVL filopodia activity that projects vegetally in the direction of migration, in a manner as to sense the environment for guidance cues. This opens the possibility that vegetally deposited chemoattractants may influence the migration of the EVL. Hence, EVL migration may not be a passive process, mediated by EVL being pulled by YSL epiboly through tight junctions. Rather, EVL epiboly is actively influenced by EVL cell motility itself, and EVL epiboly completion requires cell shape changes of the marginal EVL cells involving contractile elements. The EVL filopodia activity was also detected in MZ*spg* embryos, and therefore does not appear to account prominently for the MZ*spg* phenotype.

Our analysis of all three embryonic lineages suggests that Pou5f1 contributes to the control of epiboly progression through several mechanisms. First, some of the Pou5f1 targets mediating gastrulation defects may be activated soon after MBT via maternal message derived Pou5f1 proteins. We detected defects in tissues which downregulate *pou5f1* expression soon after MBT, including the EVL and the YCL/YSL. Targets of Pou5f1 may be responsible for proper microtubule dynamics in the YSL and YCL. The defects in formation of the contractile ring of the external YSL, and concomitant defects in coordinated marginal EVL cell shape changes may be secondary to the microtubule defects, or reflect independent activities of Pou5f1. Interestingly, both the EVL and DEL showed defects which reflect abnormal adhesiveness. The observed defects could be explained by reduced adhesiveness of MZ*spg* cells, leading in the case of the EVL to ruffle formation, and in the case of deep cells to inability to migrate effectively into the space opening between EVL and YSL as epiboly proceeds. Our time-lapse confocal analysis of living embryos shows extensive protrusive activity between DEL, EVL, and YSL, but also EVL protrusive activity probing the YSL. Together, these findings emphasize the role of cell adhesion in the control of DEL epiboly (Solnica-Krezel, 2006).

In summary, our data provide new insights into potential mechanisms of vertebrate epiboly, and suggest that Pou5f1 controls a set of migratory behaviors and adhesive properties characteristic for the very early stage of embryogenesis, when

Fig. 8. Altered adhesive properties of *pou5f1* deficient cells. Embryos were labeled by microinjection at one cell stage either with Rhodamine-dextran (MW: 10 kDa) or Alexa488-dextran (MW: 10 kDa), and primary co-cultures of dissociated and mixed sphere stage embryo cells were plated on Fibronectin/Collagen coated dishes. Volume rendering of confocal stacks of cultures: (A–C) dissociation control after plating, (D–F) after 4 h, (G–I) after 16 h incubation. (J–L) Higher magnification of cell aggregates. (J) Intermingled status of homogeneous WT–WT clusters. (K, L) Distinct subcluster formation of heterogeneous WT-MZ clusters. (M) Measurements of the percentage of intermingled clusters including standard error: WT–WT co cultures showed in 97±0% intermingled clusters, WT-MZ*spg*^{m793} co-cultures in 1.5±0.7%; $p=0.004$. (N) Predominant cell types in heterogeneous clusters. WT cells=73±12.5%; MZ*spg*^{m793} cells=13.2±2.5%; equal contribution of cell types=12.2±9.8%. In panels A, D, and G, the left (a) half images show WT control performed for the experiment in panels B, E, H, and K, and right (b) for panels C, F, I, and J. Scale bars: (A–I) 100 μm; (J–L) 50 μm.

pre- and early gastrula tissues expand and move to enable initiation of germlayer formation. Knowledge of mechanisms by which Pou5f1 controls cell adhesion and motility, and early germ layer patterning, may also contribute to a better understanding of the role of Pou5f1/Oct4 in the balance between pluripotency and carcinogenesis, as Pou5f1/Oct4 is expressed in some human tumors (Tai et al., 2005).

Acknowledgments

We thank S. Götter for fish care and help with *in vitro* fertilization; S. van der Hardt and M. Hammerschmidt for advice on primary culture; the live imaging center and R. Nitschke for confocal microscopy support; Karen Lunde for initially establishing the MZ*spg*^{m793} fish stock; and N. Kirstein for lab support. We are grateful to M. Brand for sending the *spg*^{hi349} allele. We thank A. Filippi, R. Nitschke, D. Onichtchouk, S. Ryu, and J. Schweitzer for carefully reading and commenting on the manuscript. This work was supported by DFG Collaborative Research Center grant SFB592-A3 (WD).

Appendix A. Supplementary material

Supplementary data associated with this article can be found, in the online version, at doi:10.1016/j.ydbio.2007.10.008.

References

Alarcon, V.B., Marikawa, Y., 2004. Molecular study of mouse peri-implantation development using the in vitro culture of aggregated inner cell mass. Mol. Reprod. Dev. 67, 83–90.

Amsterdam, A., Hopkins, N., 1999. Retrovirus-mediated insertional mutagenesis in zebrafish. Methods Cell Biol. 60, 87–98.

Arendt, D., Nubler-Jung, K., 1999. Rearranging gastrulation in the name of yolk: evolution of gastrulation in yolk-rich amniote eggs. Mech. Dev. 81, 3–22.

Belting, H.G., Hauptmann, G., Meyer, D., Abdelilah-Seyfried, S., Chitnis, A., Eschbach, C., Soll, I., Thisse, C., Thisse, B., Artinger, K.B., Lunde, K., Driever, W., 2001. Spiel ohne grenzen/pou2 is required during establishment of the zebrafish midbrain-hindbrain boundary organizer. Development 128, 4165–4176.

Betchaku, T., Trinkaus, J.P., 1978. Contact relations, surface activity, and cortical microfilaments of marginal cells of the enveloping layer and of the yolk syncytial and yolk cytoplasmic layers of fundulus before and during epiboly. Exp. Zool. 206, 381–426.

Betchaku, T., Trinkaus, J.P., 1986. Programmed endocytosis during epiboly of *Fundulus heteroclitus*. Am. Zool. 26, 193–199.

Boiani, M., Scholer, H.R., 2005. Regulatory networks in embryo-derived pluripotent stem cells. Nat. Rev., Mol. Cell Biol. 6, 872–884.

Boiani, M., Gentile, L., Gambles, V.V., Cavaleri, F., Redi, C.A., Scholer, H.R., 2005. Variable reprogramming of the pluripotent stem cell marker Oct4 in mouse clones: distinct developmental potentials in different culture environments. Stem Cells 23, 1089–1104.

Boyer, L.A., Lee, T.I., Cole, M.F., Johnstone, S.E., Levine, S.S., Zucker, J.P., Guenther, M.G., Kumar, R.M., Murray, H.L., Jenner, R.G., Gifford, D.K., Melton, D.A., Jaenisch, R., Young, R.A., 2005. Core transcriptional regulatory circuitry in human embryonic stem cells. Cell 122, 947–956.

Burgess, S., Reim, G., Chen, W., Hopkins, N., Brand, M., 2002. The zebrafish spiel-ohne-grenzen (spg) gene encodes the POU domain protein Pou2 related to mammalian Oct4 and is essential for formation of the midbrain and hindbrain, and for pre-gastrula morphogenesis. Development 129, 905–916.

Cha, Y.I., Kim, S.H., Sepich, D., Buchanan, F.G., Solnica-Krezel, L., DuBois, R.N., 2006. Cyclooxygenase-1-derived PGE2 promotes cell motility via the G-protein-coupled EP4 receptor during vertebrate gastrulation. Genes Dev. 20, 77–86.

Cheng, J.C., Miller, A.L., Webb, S.E., 2004. Organization and function of microfilaments during late epiboly in zebrafish embryos. Dev. Dyn. 231, 313–323.

Cooper, M.S., D'Amico, L.A., 1996. A cluster of noninvoluting endocytic cells at the margin of the zebrafish blastoderm marks the site of embryonic shield formation. Dev. Biol. 180, 184–198.

Davis, G.S., Phillips, H.M., Steinberg, M.S., 1997. Germ-layer surface tensions and "tissue affinities" in *Rana pipiens* gastrulae: quantitative measurements. Dev. Biol. 192, 630–644.

Gard, D.L., 1991. Organization, nucleation, and acetylation of microtubules in *Xenopus laevis* oocytes: a study by confocal immunofluorescence microscopy. Dev. Biol. 143, 346–362.

Goto, T., Davidson, L., Asashima, M., Keller, R., 2005. Planar cell polarity genes regulate polarized extracellular matrix deposition during frog gastrulation. Curr. Biol. 15, 787–793.

Hochedlinger, K., Yamada, Y., Beard, C., Jaenisch, R., 2005. Ectopic expression of Oct-4 blocks progenitor-cell differentiation and causes dysplasia in epithelial tissues. Cell 121, 465–477.

Howley, C., Ho, R.K., 2000. mRNA localization patterns in zebrafish oocytes. Mech. Dev. 92, 305–309.

Huang, H., Lu, F.I., Jia, S., Meng, S., Cao, Y., Wang, Y., Ma, W., Yin, K., Wen, Z., Peng, J., Thisse, C., Thisse, B., Meng, A., 2007. Amotl2 is essential for cell movements in zebrafish embryo and regulates c-Src translocation. Development 134, 979–988.

Imamura, Y., Itoh, M., Maeno, Y., Tsukita, S., Nagafuchi, A., 1999. Functional domains of alpha-catenin required for the strong state of cadherin-based cell adhesion. J Cell Biol. 144, 1311–1322.

Ivanova, N., Dobrin, R., Lu, R., Kotenko, I., Levorse, J., DeCoste, C., Schafer, X., Lun, Y., Lemischka, I.R., 2006. Dissecting self-renewal in stem cells with RNA interference. Nature 442, 533–538.

Jacinto, A., Wood, W., Woolner, S., Hiley, C., Turner, L., Wilson, C., Martinez-Arias, A., Martin, P., 2002a. Dynamic analysis of actin cable function during *Drosophila* dorsal closure. Curr. Biol. 12, 1245–1250.

Jacinto, A., Woolner, S., Martin, P., 2002b. Dynamic analysis of dorsal closure in *Drosophila*: from genetics to cell biology. Dev. Cell 3, 9–19.

Jiang, W., Hunter, T., 1998. Analysis of cell-cycle profiles in transfected cells using a membrane-targeted GFP. Biotechniques. 24, 349–50, 352, 354.

Kane, D.A., Kimmel, C.B., 1993. The zebrafish midblastula transition. Development 119, 447–456.

Kane, D.A., Hammerschmidt, M., Mullins, M.C., Maischein, H.-M., Brand, M., van-Eeden, F.J.M., Furutani-Seiki, M., Granato, M., Haffter, P., Heisenberg, C.-P., Jiang, Y.-J., Kelsh, R.N., Odenthal, J., Warga, R.M., Nüsslein-Volhard, C., 1996a. Early arrest mutants in zebrafish. Development 123, 57–66.

Kane, D.A., Maischein, H.M., Brand, M., van Eeden, F.J., Furutani-Seiki, M., Granato, M., Haffter, P., Hammerschmidt, M., Heisenberg, C.P., Jiang, Y.J., Kelsh, R.N., Mullins, M.C., Odenthal, J., Warga, R.M., Nusslein-Volhard, C., 1996b. The zebrafish early arrest mutants. Development 123, 57–66.

Kane, D.A., McFarland, K.N., Warga, R.M., 2005. Mutations in half baked/E-cadherin block cell behaviors that are necessary for teleost epiboly. Development 132, 1105–1116.

Kehler, J., Tolkunova, E., Koschorz, B., Pesce, M., Gentile, L., Boiani, M., Lomeli, H., Nagy, A., McLaughlin, K.J., Scholer, H.R., Tomilin, A., 2004. Oct4 is required for primordial germ cell survival. EMBO Rep. 5, 1078–1083.

Kimmel, C.B., Ballard, W.W., Kimmel, S.R., Ullmann, B., Schilling, T.F., 1995. Stages of embryonic development of the zebrafish. Dev. Dyn. 203, 253–310.

Koeppen, M., Fernandez, B.G., Carvalho, L., Jacinto, A., Heisenberg, C.P., 2006. Coordinated cell-shape changes control epithelial movement in zebrafish and *Drosophila*. Development 133, 2671–2681.

Leskow, F.C., Holloway, B.A., Wang, H., Mullins, M.C., Kazanietz, M.G., 2006. The zebrafish homologue of mammalian chimerin Rac-GAPs is implicated in epiboly progression during development. Proc. Natl. Acad. Sci. U. S. A. 103, 5373–5378.

Loh, Y.H., Wu, Q., Chew, J.L., Vega, V.B., Zhang, W., Chen, X., Bourque, G., George, J., Leong, B., Liu, J., Wong, K.Y., Sung, K.W., Lee, C.W., Zhao, X.D., Chiu, K.P., Lipovich, L., Kuznetsov, V.A., Robson, P., Stanton, L.W., Wei, C.L., et al., 2006. The Oct4 and Nanog transcription network regulates pluripotency in mouse embryonic stem cells. Nat. Genet. 38, 431–440.

Lunde, K., Belting, H.G., Driever, W., 2004. Zebrafish pou5f1/pou2, homolog of mammalian Oct4, functions in the endoderm specification cascade. Curr. Biol. 14, 48–55.

McFarland, K.N., Warga, R.M., Kane, D.A., 2005. Genetic locus half baked is necessary for morphogenesis of the ectoderm. Dev. Dyn. 233, 390–406.

Mintzer, K.A., Lee, M.A., Runke, G., Trout, J., Whitman, M., Mullins, M.C., 2001. Lost-a-fin encodes a type I BMP receptor, Alk8, acting maternally and zygotically in dorsoventral pattern formation. Development 128, 859–869.

Montero, J.A., Kilian, B., Chan, J., Bayliss, P.E., Heisenberg, C.P., 2003. Phosphoinositide 3-kinase is required for process outgrowth and cell polarization of gastrulating mesendodermal cells. Curr. Biol. 13, 1279–1289.

Mullins, M.C., Hammerschmidt, M., Kane, D.A., Odenthal, J., Brand, M., van Eeden, F.J., Furutani-Seiki, M., Granato, M., Haffter, P., Heisenberg, C.P., Jiang, Y.J., Kelsh, R.N., Nusslein-Volhard, C., 1996. Genes establishing dorsoventral pattern formation in the zebrafish embryo: the ventral specifying genes. Development 123, 81–93.

Myers, D.C., Sepich, D.S., Solnica-Krezel, L., 2002. Bmp activity gradient regulates convergent extension during zebrafish gastrulation. Development 1–18.

Nichols, J., Zevnik, B., Anastassiadis, K., Niwa, H., Klewe-Nebenius, D., Chambers, I., Scholer, H., Smith, A., 1998. Formation of pluripotent stem cells in the mammalian embryo depends on the POU transcription factor Oct4. Cell 95, 379–391.

Niwa, H., 2007. How is pluripotency determined and maintained? Development 134, 635–646.

Niwa, H., Miyazaki, J.I., Smith, A.G., 2000. Quantitative expression of Oct-3/4 defines differentiation, dedifferentiation or self-renewal of ES cells. Nat. Genet. 24, 372–376.

Ovitt, C.E., Scholer, H.R., 1998. The molecular biology of Oct-4 in the early mouse embryo. Mol. Hum. Reprod. 4, 1021–1031.

Owens, D.W., McLean, G.W., Wyke, A.W., Paraskeva, C., Parkinson, E.K., Frame, M.C., Brunton, V.G., 2000. The catalytic activity of the Src family kinases is required to disrupt cadherin-dependent cell-cell contacts. Mol Biol Cell. 11, 51–64.

Pan, G.J., Chang, Z.Y., Scholer, H.R., Pei, D., 2002. Stem cell pluripotency and transcription factor Oct4. Cell Res. 12, 321–329.

Pesce, M., Scholer, H.R., 2001. Oct-4: gatekeeper in the beginnings of mammalian development. Stem Cells 19, 271–278.

Pesce, M., Gross, M.K., Scholer, H.R., 1998. In line with our ancestors: Oct-4 and the mammalian germ. BioEssays 20, 722–732.

Reim, G., Brand, M., 2006. Maternal control of vertebrate dorsoventral axis formation and epiboly by the POU domain protein Spg/Pou2/Oct4. Development 133, 2757–2770.

Reim, G., Mizoguchi, T., Stainier, D.Y., Kikuchi, Y., Brand, M., 2004. The POU domain protein spg (pou2/Oct4) is essential for endoderm formation in cooperation with the HMG domain protein casanova. Dev. Cell 6, 91–101.

Schier, A.F., Joyner, A.L., Lehmann, R., Talbot, W.S., 1996. From screens to genes: prospects for insertional mutagenesis in zebrafish. Genes Dev. 10, 3077–3080.

Shih, J., Fraser, S.E., 1996. Characterizing the zebrafish organizer: micro-surgical analysis at the early-shield stage. Development 122, 1313–1322.

Shimizu, T., Yabe, T., Muraoka, O., Yonemura, S., Aramaki, S., Hatta, K., Bae, Y.K., Nojima, H., Hibi, M., 2005. E-cadherin is required for gastrulation cell movements in zebrafish. Mech. Dev. 122, 747–763.

Solnica-Krezel, L., 2005. Conserved patterns of cell movements during vertebrate gastrulation. Curr. Biol. 15, R213–R228.

Solnica-Krezel, L., 2006. Gastrulation in zebrafish-all just about adhesion? Curr. Opin. Genet. Dev. 16, 433–441.

Solnica-Krezel, L., Driever, W., 1994. Microtubule arrays of the zebrafish yolk cell: organization and function during epiboly. Development 120, 2443–2455.

Solnica-Krezel, L., Stemple, D.L., Driever, W., 1995. Transparent things: cell fates and cell movements during early embryogenesis of zebrafish. BioEssays 17, 931–939.

Strahle, U., Jesuthasan, S., 1993. Ultraviolet irradiation impairs epiboly in zebrafish embryos: evidence for a microtubule-dependent mechanism of epiboly. Development 119, 909–919.

Tai, M.H., Chang, C.C., Kiupel, M., Webster, J.D., Olson, L.K., Trosko, J.E., 2005. Oct4 expression in adult human stem cells: evidence in support of the stem cell theory of carcinogenesis. Carcinogenesis 26, 495–502.

Takahashi, K., Yamanaka, S., 2006. Induction of pluripotent stem cells from mouse embryonic and adult fibroblast cultures by defined factors. Cell 126, 663–676.

Takeda, H., Matsuzaki, T., Oki, T., Miyagawa, T., Amanuma, H., 1994. A novel POU domain gene, zebrafish pou2: expression and roles of two alternatively spliced twin products in early development. Genes Dev. 8, 45–59.

Takeda, H., Nagafuchi, A., Yonemura, S., Tsukita, S., Behrens, J., Birchmeier, W., Tsukita, S., 1995. V-src kinase shifts the cadherin-based cell adhesion from the strong to the weak state and beta catenin is not required for the shift. J Cell Biol. 131, 1839–1847.

von der Hardt, S., Bakkers, J., Inbal, A., Carvalho, L., Solnica-Krezel, L., Heisenberg, C.P., Hammerschmidt, M., 2007. The Bmp gradient of the zebrafish gastrula guides migrating lateral cells by regulating cell–cell adhesion. Curr. Biol. 17, 475–487.

Wallingford, J.B., 2005. Vertebrate gastrulation: polarity genes control the matrix. Curr. Biol. 15, R414–R416.

Westerfield, M., 1994. The Zebrafish Book. University of Oregon Press, Eugene.